OVERCOMING CHALLENGES IN SURFACE-ENHANCED RAMAN SPECTROSCOPIC DETECTION: APPROACHES FOR QUANTITATIVE ANALYSIS OF REACTION KINETICS AND INCREASED CONFIDENCE OF SUBSTANCE IDENTIFICATION

A Dissertation

by

JOSHUA DAVID WEATHERSTON

Submitted to the Office of Graduate and Professional Studies of
Texas A&M University
in partial fulfillment of the requirements for the degree of

DOCTOR OF PHILOSOPHY

Chair of Committee,	Hung-Jen Wu
Committee Members,	Arul Jayaraman
	Katy C. Kao
	Gerard L. Coté
Head of Department,	Muhammad N. Karim

May 2019

Major Subject: Chemical Engineering

ABSTRACT

Surface-Enhanced Raman Spectroscopy (SERS) is a modification to traditional Raman spectroscopy (RS) which inherits the high specificity of RS while featuring greatly improved sensitivity. As a result, SERS spectroscopy is capable of uniquely identifying low-abundance chemical species within complex samples. However, due to challenges in implementing SERS spectroscopy, it has not found widespread use in sensing applications. The focus of this body of research is to overcome three significant challenges to the viability of SERS, namely: (1) the poor signal reproducibility leads to unsatisfactory quantitative analysis, (2) spectral overlap and interference confounds the interpretation of complex samples, and (3) additional sample preparation requirements complicate the method, making it less suitable for many applications. These challenges were addressed through the design and implementation of specialized SERS substrates and assays.

To improve the quantitative capabilities of SERS spectroscopy, an assay was developed based on a SERS-active probe functionalized with an internal calibration standard. As a result, despite significant variability in the absolute signal intensity, the self-calibrated relative signal intensity remained stable. The assay was verified by observing the SERS spectral shift throughout an aldol condensation reaction and calculating the kinetic rate constants for the reaction, which compared favorably with literature values.

To simplify SERS spectral interpretation, we introduced nanopaper, consisting of glass fiber paper decorated with silver nanoparticles. This dual-function material can be used as a SERS substrate as well as a stationary phase for paper chromatography separation, which simplifies spectral analysis by reducing the complexity of the sample. Both functions were

simple to implement, requiring minimal sample preparation. Nanopaper performance was verified by successfully separating and detecting a mixture of organic dyes on nanopaper. The utility of coupling paper chromatography with SERS was further demonstrated by identifying the carotenoids lycopene and β-carotene, which have practically indistinguishable SERS spectra, in vegetable extracts. The approaches detailed herein mitigate the shortcomings of SERS methods without compromising the inherent strengths of the technique, facilitating access to a powerful analytical technique for researchers in diverse disciplines.

ACKNOWLEDGEMENTS

I would like to thank my committee chair, Dr. Wu, and my committee members, Dr. Jayaraman, Dr. Kao, and Dr. Coté, for their guidance and support throughout the course of this research.

I would like to express my gratitude and appreciation for my friends and colleagues, who were always ready to let me bounce ideas off of them and – all too often – to help me find all the things I misplaced in the lab (usually right in front of myself). My thanks also go to the department faculty and staff for making my time at Texas A&M University a great experience.

CONTRIBUTORS AND FUNDING SOURCES

This work was supported by a dissertation committee consisting of Professor Hung-Jen Wu and Professors Arul Jayaraman and Katy C. Kao of the Department of Chemical Engineering and Professor Gerard L. Coté of the Department of Biomedical Engineering.

All experiments were conceived and designed by myself and Hung-Jen Wu of the Department of Chemical Engineering. Chapter II experiments were performed by myself and Nolan C. Worstell of the Department of Chemical Engineering, and Chapter III experiments were performed by myself and Ricci Kirsten O. Seguban of the Department of Chemical Engineering. Experimental results were analyzed by myself and Hung-Jen Wu of the Department of Chemical Engineering. Chapters II and III were written by myself and Hung-Jen Wu of the Department of Chemical Engineering. The contributed reagents/materials/analytical tools for Chapters II and III were from myself and Hung-Jen Wu of the Department of Chemical Engineering.

This work was supervised by a dissertation committee consisting of Professor Hung-Jen Wu and Professors Arul Jayaraman and Katy C. Kao of the Department of Chemical Engineering and Professor Gerard L. Coté of the Department of Biomedical Engineering. Graduate study was supported by a fellowship from Texas A&M.

NOMENCLATURE

CE	chemical enhancement
CR	cresol red
CV	crystal violet
DFT	density functional theory
EDX	energy dispersive X-ray spectroscopy
EM	electromagnetic enhancement
FEM	finite element method
HAADF-STEM	high-angle annular dark field - scanning transmission electron microscope
IR	infrared absorption spectroscopy
IS	internal calibration standard
LC-MS	liquid chromatography - mass spectrometry
MO	methyl orange
MP	4-mercaptophenol
MTBH	4-(methylthio)benzaldehyde
NTP	4-nitrothiophenol
PC-SERS	paper chromatography - surface-enhanced Raman spectroscopy
R6G	rhodamine 6G
RS	Raman spectroscopy
SEM	scanning electron microscope
SERS	surface-enhanced Raman spectroscopy
TEM	transmission electron microscope

TABLE OF CONTENTS

Page

LIST OF FIGURES

Page

CHAPTER I

INTRODUCTION

Spectroscopy, the study of matter by observing its interaction with radiation, is one of our primary tools in understanding the world around us, from the atomic scale to the astronomic scale.[1] Because the identification and characterization of chemical substances play such vital roles in scientific and industrial pursuits, spectroscopic methods which provide information at the molecular level are particularly valuable. Vibrational spectroscopies, comprising infrared absorption spectroscopy (IR) and Raman spectroscopy (RS), provide such analysis by probing the energies of molecular vibrational modes. Molecular species have unique combinations of vibrational energies, and those energies are sensitive to the molecule's environment, so vibrational spectroscopy can provide a wealth of information about the composition and physical state of a sample.

Raman spectroscopy in particular has received recent attention, largely owing to the development of surface-enhanced Raman spectroscopy (SERS). SERS can boost Raman signal by many orders of magnitude, allowing detection of extremely dilute chemical species. SERS has changed the landscape of Raman spectroscopy, revitalizing this field of study and extending its potential for practical applications. However, despite some clear advantages over RS, SERS is still in its developmental stage; its high sensitivity and specificity is counterbalanced by difficulties with reproducibility, portability, and selectivity which must be addressed for successful implementation in sensing applications.

Raman Spectroscopy

As a molecular detection method, Raman spectroscopy is fundamentally versatile; virtually all materials will produce a Raman spectrum.[2] Consequently, its applications are too exhaustive to reasonably list. In a review on recent advances in Raman spectroscopy, W. Kiefer details applications in such diverse fields as biosciences, art and archeology, nanomaterials, forensic science, pharmaceutical studies, solid state physics, phase transition analysis, and many others.[3]

Raman spectroscopy relies on Raman scattering, an inelastic light scattering phenomenon first demonstrated in 1928 by C. V. Raman.[4] In Raman scattering, incident light experiences frequency shifts due to its interaction with matter. This frequency shift, called Raman shift, corresponds to the energy of molecular vibrations within the sample. Raman spectroscopy is the process of producing Raman-shifted photons, sorting those photons by energy, and then counting them. The result is a Raman spectrum, which shows the intensity of inelastically scattered light as a function of the Raman shift. A wealth of information about a system can be gleaned from its Raman spectrum. The unique pattern of spectral peaks indicates a unique combination of vibrational energies, allowing "fingerprint" identification of substances. Furthermore, molecular vibrational energies are influenced by the molecular environment, meaning subtle shifts in peak locations can further characterize the system, revealing bond strains, inter- and intramolecular interactions, protonation state, and effects from temperature and pressure, among others.

Theory and instrumentation of Raman spectroscopy

When a photon interacts with a molecule, there are several possible consequences (Figure 1). If the photon energy matches the energy difference between two molecular states, it may be absorbed, promoting the molecule to an excited state. For example, the energies of molecular

vibrational modes typically correspond to energies found in the infrared spectrum of light; IR spectroscopy takes advantage of this, measuring the absorbance of infrared wavelengths to identify molecular vibrational energies.[2]

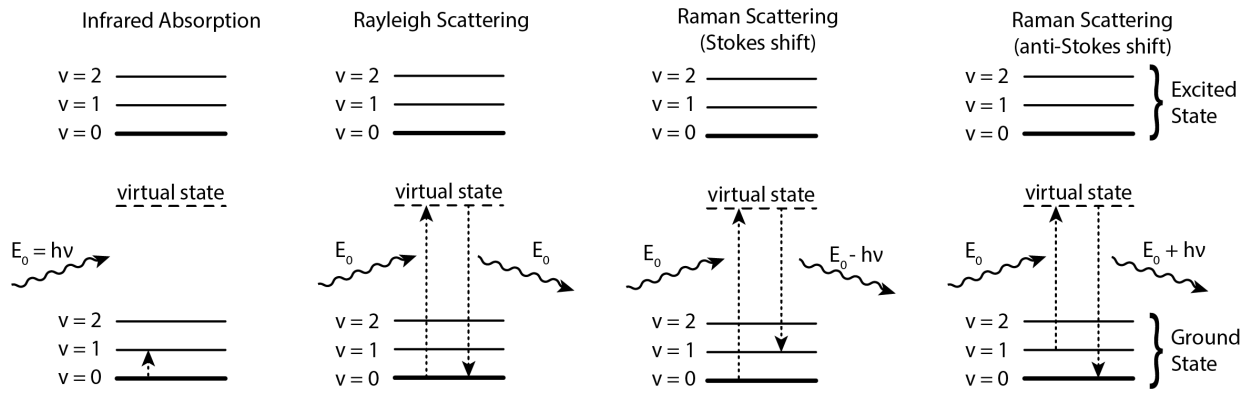

Figure 1. Simplified Jablonski diagram demonstrating radiative energy transitions involved with vibrational spectroscopies.

If the energy of the incident photon does not correspond to the energy of a molecular transition, it may undergo a scattering process. In optical scattering, the photon is absorbed through a transition to a virtual electronic state, and a photon is also simultaneously emitted, collapsing the molecule back to the ground electronic state. This virtual state does not need to coincide with a real electronic state; therefore, scattering can occur at all frequencies of incident light. Scattering can be either elastic or inelastic. Elastic scattering is called Rayleigh scattering, and involves no energy transfer to or from the molecule; the scattered photon has the same energy as the incident photon. Inelastic scattering is called Raman scattering, and entails energy transfer between photon and molecule, producing a scattered photon with different energy (and therefore a different frequency) than the incident photon. A photon gains energy if the molecule

was in an excited vibrational state before the scattering event (anti-Stokes shift), but loses energy if the molecule was initially in the ground state (Stokes shift).[2]

The great majority of scattering that occurs is Rayleigh scattering, which gives no information about molecular energy states. The Raman scattering power is proportional to the number of scatterers sampled, the power density of incident light, and a quantity called the Raman cross section. Each vibrational mode has a Raman cross section which is dependent on the incident light frequency, the molecule's spatial orientation with respect to the incident light, and the change in molecular polarizability induced by the vibration.[2,5] Compared to many other optical processes, Raman cross sections are small; for example, typical Raman cross sections are ~14 orders of magnitude smaller than those of fluorescence.[5]

To compensate for the low Raman cross section and achieve sufficient sensitivity for reliable detection, high incident power density is required. Therefore, conventional Raman instrumentation usually requires a high-powered monochromatic laser source focused on a sample through microscope optics. As scattering occurs, the scattered light is collected by optics and passed through a filter that rejects Rayleigh scattering, effectively eliminating the incident frequency, while allowing Raman scattered light to proceed. A spectrograph then separates the signal into its component frequencies and records the intensity of each frequency (Figure 2). Intensity is plotted vs. Raman shift (in units of cm^{-1}) to yield a Raman spectrum.

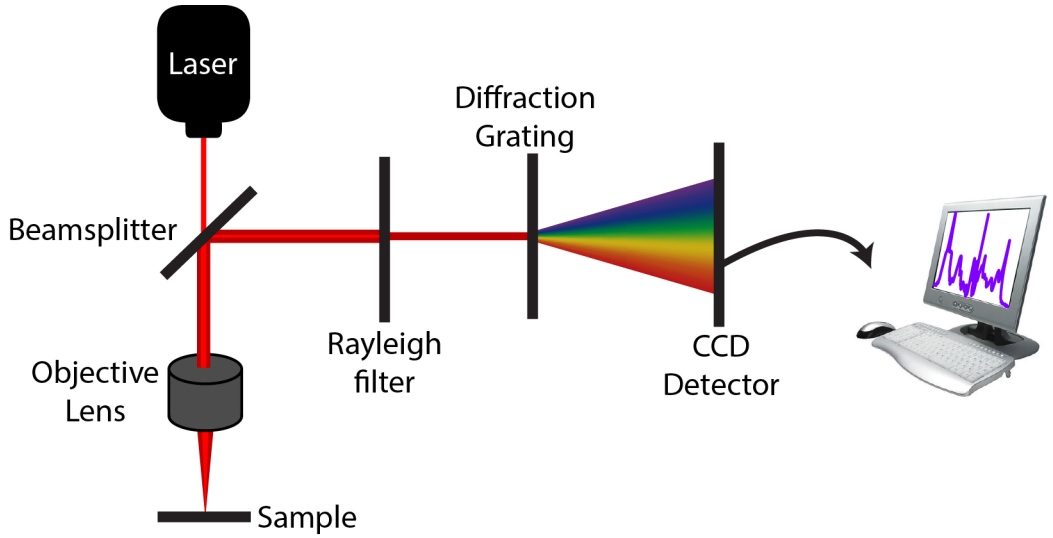

Figure 2. Schematic of Raman Spectroscopy instrumentation.

Raman spectroscopy advantages and disadvantages

Raman spectroscopy has many attractive features. As previously mentioned, it is a highly versatile tool and it yields great quantities of information about the system under study. Because it is a remote sensing platform, it is usually considered a non-invasive and non-destructive method; samples can be reused and remeasured.[6] RS can easily penetrate water and glass, allowing detection in sealed vessels and aqueous environments. The introduction of portable Raman spectrometers opens up numerous potential applications, making it ideal for on-site work in diverse disciplines such as law enforcement, forensic science, point-of-care medical testing, and many more. Because Raman scattering is proportional to the number of scatterers in the collection volume, RS is well suited to quantitative analysis.[7]

Raman gives information that is complementary to that of IR. This is because the selection rules for absorption and scattering processes are different. Vibrations involving asymmetrical bonds and polar groups exhibit strong IR absorption, while vibrations involving symmetrical bonds and nonpolar groups exhibit strong Raman scattering. Peaks that are strong in

RS may be weak or entirely absent in IR; the reverse also holds true.[8] An important consequence of this is that RS is compatible with water, whereas water absorbs strongly in much of the infrared spectral region.[9] Sample preparation for RS is also usually much simpler than it is for IR; as a non-absorption process, samples need not be transparent and due to the microscope optics, sample size could be as small as a few microns.[6]

RS possesses several advantages over fluorescence spectroscopy.[2] Its high specificity is superior to that of fluorescence due to the unique "fingerprint" Raman spectrum. RS is also a direct measurement method and can also be performed with virtually any molecule without need for labelling. In contrast, fluorescence necessitates the use of a good fluorophore, limiting experimental options. RS can theoretically be used with any excitation frequency (although practically it is limited based on commercial availability and optical transmission considerations), while fluorescence excitation must be tuned to the fluorophore used. As a direct sensing method, RS can detect multiple species at once, and quantify their relative abundance. To achieve such multiplexed detection with fluorescence, multiple fluorophores are required which have limited spectral overlap. Since fluorescence peaks are much broader than RS peaks, this means that only a few species can be monitored at a time. Finally, RS is not subject to photobleaching, which is a major experimental concern in fluorescence measurements.

Despite many advantages over similar analytical methods, RS has distinct disadvantages. The overwhelming shortcoming is the extremely weak signal. This makes the method unsuited to applications that require high sensitivity; due to the relatively massive amount of Rayleigh scattering, the signal to noise ratio for dilute samples is not desirable. This results in the necessity for long collection times and highly concentrated samples, especially for analytes with small Raman cross sections. This issue is further complicated by background fluorescence. Like

Raman scattering, fluorescence emission involves a frequency shift in the photon. Since only incident frequency photons are rejected by the Rayleigh filter, fluorescent signal is fully detected by the spectrograph. This results in extremely broad, obscuring fluorescence peaks in the Raman spectrum. Because fluorescence cross sections are so much larger than Raman cross sections, even weakly fluorescent materials or minute traces of fluorescent impurities can completely obliterate the relatively weak Raman signal. This issue can be mitigated by judicious selection of Raman excitation frequency to minimize fluorescent contributions and by intentionally photobleaching the sample through extended laser exposure. In many cases, however, fluorescence background contributions partially or totally obscure the Raman spectrum. This obscuring phenomenon is not an issue with IR measurements.

Surface-Enhanced Raman Spectroscopy (SERS)

In the early 1970s, it was thought that the weakness of Raman signal and the poor capabilities of Raman instrumentation would make RS infeasible for monolayer adsorption studies.[10] However, in 1974, Fleischmann et al. measured the Raman spectrum of pyridine adsorbed on electrochemically roughened silver electrodes.[11] This is now known as the first reported incidence of SERS, but at the time it was explained by an increase in the number of molecules caused by increased surface area from the roughening.[12] Subsequent studies soon demonstrated that this effect could not account for such a dramatic increase in signal, and some other surface effect was causing signal enhancement by a factor of $\sim 10^6$.[13,14] This ignited decades of study in the field of SERS.[15]

SERS is a surface effect that vastly increases the intensity of Raman scattering from a molecule (the SERS probe) when it is adsorbed on a nanostructured metallic surface (the SERS substrate). The great value in SERS is that it inherits the advantages of RS while overcoming

some of the major limitations of RS. As a vibrational spectroscopy, it provides unique, information-rich spectra complimentary to that obtained from IR. SERS also maintains compatibility with aqueous measurement environments, as well as flexibility in selection of probe molecules and excitation frequencies. It offers an improvement over RS, effectively overcoming the largest disadvantage of RS by increasing the sensitivity to allow ultrasensitive chemical analysis. Under certain conditions, Raman signal enhancement by a factor of up to $\sim 10^{14}$–10^{15} can be achieved, allowing the detection of single-molecule Raman signals of comparable intensity to single-molecule fluorescence.[16,17] Furthermore, the metallic surfaces necessary to SERS tend to quench the fluorescence interference that afflicts RS.[5]

SERS enhancement mechanisms

The SERS enhancement factor is the intensity ratio of a SERS peak to its corresponding RS peak (assuming equal excitation energy, number of molecules sampled, etc.). The physical mechanism behind the SERS effect is thought to have two contributing factors, termed electromagnetic (EM) enhancement and chemical enhancement (CE). EM enhancement is generally accepted to be the primary contributor while chemical enhancement CE contributes in a much smaller way (its very existence is somewhat controversial).[18]

CE is the result of an alteration in the Raman cross section of the adsorbate molecule due to the formation of an adsorbate-metal complex.[18] The mechanism of CE is not well understood, but the most commonly cited theory is that a charge-transfer state is created between the adsorbate molecule and the metal substrate, opening a pathway for resonant excitation.[19] The CE increases signal by a factor of $\sim 10^2$, but it only contributes if the molecule is directly adsorbed to the surface.[5]

EM enhancement makes up the remainder of the total enhancement factor. Depending on the design of the SERS substrate, EM enhancement can increase Raman signal by a factor of 10^1–10^{13}. Whereas CE is dependent on the interaction between the surface and the adsorbed molecule, the EM mechanism is rooted in the interaction between the surface and the incident light. When EM radiation interacts with the surface, it induces collective oscillations in the material's conduction band electrons. This oscillation, called a surface plasmon, generates intense but highly localized electric fields which extend a short distance into the surrounding environment (≤10 nm from the surface). The magnitude of these fields is dependent on the size, shape, and spacing of the nanostructures, the dielectric properties of the surface and its environment, and the frequency of the incident EM radiation. The increase in Raman signal due to the EM mechanism is approximately proportional to the fourth power of the electric field magnitude ratio of locally amplified field to background field.[*] Unlike the CE mechanism, EM enhancement does not require an adsorption bond; however, because electric fields are only amplified within several nm of the surface, the Raman probe must still be very close to the surface.

Design of SERS substrates

The surface involved in SERS is called the SERS substrate. SERS is fundamentally a surface effect, but not just any surface will produce significant signal enhancement. A well-designed SERS substrate is a material that generates a large number of intense localized electric fields when irradiated, taking advantage of the EM enhancement mechanism. Design considerations include the composition, size, shape, and large-scale configuration of the material.

[*] RS/SERS involves simultaneous absorption and emission events, each of which is proportional to the power density of its electromagnetic environment. This power density is in turn proportional to the squared magnitude of the electric field, resulting in the so-called "fourth-power relation".

Most substrates are composed of coinage metals (Ag, Au, Cu) because their dielectric properties enable large EM enhancements at the visible and NIR excitations typically used in SERS. Of these, Ag has the largest potential for enhancement, followed by Au and then Cu.[20] The size of surface features within the substrate should be on the nanoscale, because particles smaller than the excitation wavelength can generate resonant localized surface plasmons, contributing to the EM enhancement of the substrate.[21] Shape also contributes to enhancement; sharp surface features like edges and corners tend to "concentrate" the electric fields, increasing EM enhancement.[22,23] Interfeature spacing is also extremely important in SERS subtrates. When the enhanced electric fields from multiple surfaces overlap, the resulting "hot-spot" can yield particularly impressive enhancement.[18]

Formats for SERS substrates fall into three general categories: nanoparticles sols, immobilized nanoparticle films, and direct nanostructure fabrication onto solid surfaces.[24] Nanoparticle substrates are useful because a wide variety of stable, scalable protocols are available to synthesize particles of virtually every size and shape. Furthermore, it is possible to tune interparticle spacing in both sols and films, allowing control over the density of SERS hot-spots.[23] Nanostructure arrays fabricated via nanolithography or template techniques have an advantage in uniformity and reproducibility, but such substrates are much more difficult to synthesize, requiring specialized equipment and technical skills; the synthesis is also high cost and low throughput.[23,25,26]

Challenges to implementing SERS

Despite its great advantages, SERS introduces some additional challenges to practical implementation in chemical sensing applications. The most obvious is the requirement to achieve intimate contact between the probe molecule and a SERS substrate, which complicates sample

preparation compared to RS experiments.[26] First, a substrate must be synthesized or purchased. Then, the sample must be introduced to the substrate and allowed sufficient time to adsorb. In scenarios with more than one probe species, competing or selective adsorption may cause the results to be misleading. One or more washing steps may be needed to remove excess analytes and the measurement itself can be more difficult to perform due to the heterogeneous nature of the sample. SERS substrates can also be delicate; silver readily oxidizes in many environments, resulting in decreased sensitivity over time. The increased sample preparation requirements with SERS are particularly problematic for field-work applications where portability and simplicity are vital.

Another challenge is the difficulty in obtaining reliable quantitative results. SERS signal intensity is highly dependent on substrate morphology, so it is difficult to determine if variation in spectral intensity results from true variation in the sample composition or from variation in the substrate morphology (i.e. aggregation in a colloid or heterogeneity across a solid surface).[27] In theory, this issue could be resolved by engineering highly uniform substrates, but in practice this is difficult to achieve.[28] In patterned films, the uniformity of periodic metallic structures can influence the SERS effect. In nanoparticle colloids, particle sedimentation and aggregation can change the average interparticle distance between nanoparticles, modulating the strength of SERS signals. In addition, the EM enhancement is dependent on the local dielectric environment, which can change for reacting systems over time. Therefore, quantitative detection must be designed to achieve quantitative SERS.

Another difficulty in using SERS as a detection tool lies in the interpretation of spectral data. The great advantage of RS and SERS – the wealth of information from vibrational energy levels – can sometimes be both harm and help. Depending on the sample, spectral interpretation

can range from straightforward to highly challenging. As the number of chemical species in a sample increases, SERS peaks are more likely to overlap, confounding features that would be clearly resolved in a pure sample. While peak-fitting procedures can help resolve overlapping peaks, such procedures are highly sensitive to user input parameters, and depend on being able to determine the number of hidden peaks in a spectral region. More sophisticated statistical methods, such as principal component analysis (PCA) or hierarchical cluster analysis (HCA), may also be used to resolve a complex spectrum into its contributing component spectra. These methods are useful, but require large datasets and reference libraries to be successful.[29] When multiple probe species are present, deconvoluting the mixture spectrum to identify the components can be a daunting task.

Overview of following chapters

In subsequent chapters, I will detail the specific approaches I have used in my research to resolve difficulties with SERS implementation. Chapter II focuses on the challenge of achieving quantitative SERS. Specifically, it demonstrates a simple approach to reliably and quantitatively determine kinetic parameters in a reacting system. Chapter III focuses on the challenge of interpreting SERS spectra. Rather than introducing complicated statistical analyses, the spectra themselves are simplified through chromatography separation that occurs on the SERS substrate itself. Both Chapters II and III give insight into designing SERS substrates with scalable, simple production, with an emphasis on easing and streamlining sample preparation. Finally, Chapter IV concludes the main portion of this dissertation through summary and an explanation of the future research prospects for the work contained herein.

CHAPTER II

QUANTITATIVE SURFACE-ENHANCED RAMAN SPECTROSCOPY FOR KINETIC ANALYSIS OF ALDOL CONDENSATION USING AG–AU CORE–SHELL NANOCUBES[*]

Chapter Summary

Surface-enhanced Raman spectroscopy (SERS) is a powerful tool with high potential for multiplexed detection of dilute analytes. However, quantitative SERS of kinetic assays can be difficult due to the variation in enhancement factors caused by changing reaction conditions. We report a method for quantitative SERS kinetic analysis using colloidal Ag–Au core–shell nanocubes (Ag@AuNCs) as the SERS substrate. This substrate is mass producible, possesses large SERS enhancement, and is resistant to degradation in most environments. The SERS enhancement of the Ag@AuNCs was evaluated both experimentally and computationally. Quantitation was achieved by covalently attaching a non-reactive internal standard (IS) to substrate surfaces and normalizing SERS spectra to the IS signal. We demonstrated that IS normalization corrects for temporal variations in enhancement factor and particle concentration. Quantitation was demonstrated by monitoring the base-catalyzed aldol condensation of surface-bound 4-(methylthio)benzaldehyde with free acetone. The kinetic model of this reaction was fitted to IS normalized SERS data, resulting in kinetic parameters that agreed well with published values. This SERS platform is a robust and sensitive method for quantitative analysis of kinetic assays, with potential applications in many fields.

---

[*] Reproduced with permission from Weatherston, J. D., Worstell, N. C. & Wu, H.-J. Quantitative surface-enhanced Raman spectroscopy for kinetic analysis of aldol condensation using Ag-Au core-shell nanocubes. *Analyst 141*, 6051-6060, doi:10.1039/C6AN01098A (2016).

Introduction

Raman spectroscopy is an analytical technique which provides fingerprint information capable of directly identifying chemical species. Surface enhanced Raman Spectroscopy (SERS) is a surface phenomenon that amplifies the inherently weak Raman scattering signal of molecules adsorbed on metal surfaces by many orders of magnitude.[20,30,31] SERS advantages include large signal enhancement, fingerprint chemical identification, and inherent suitability for aqueous measurements. These advantages make SERS an effective tool for qualitative detection of dilute analytes in complex media. SERS has great potential for sensing applications in many fields, including biological detection, environmental toxicology, reaction analysis, and forensic science.[32-34] However, quantitative SERS remains challenging because the signal strength can be confounded by variable signal enhancements.[35]

The SERS effect is induced primarily by the amplified electromagnetic (EM) field near nanostructured metal surfaces. EM enhancement is a near field effect and is particularly large in hot spots – nanoscale gaps between surfaces. Because of this, SERS-active substrates have been designed either as solid films of patterned metallic structures[36] or as nanoparticle colloids.[37] Both types of substrate provide large signal enhancement, but they also suffer from variability in enhancement. In patterned films, the uniformity of periodic metallic structures can influence the SERS effect. In nanoparticle colloids, particle sedimentation and aggregation can change the average interparticle distance between nanoparticles, modulating the strength of SERS signals. In addition, the SERS effect is dependent on the local dielectric environment, which can change as a reaction mixture evolves with time. Therefore, quantitative detection must be designed to account for the changing environment of a kinetic study.

To overcome these barriers in SERS quantification, we report a method in which a colloidal suspension of SERS-active core (silver)–shell (gold) nanocubes (Ag@AuNCs) is used in conjunction with an internal standard (IS) for quantitative signal calibration. The enhancing properties of silver and the easy, scalable synthesis of highly structured, monodisperse silver nanoparticles offer an ideal SERS-active substrate. A thin gold film provides a protective coating over the silver core in order to maintain the large SERS enhancement despite harsh environments (see schematic in Figure 3). The Ag@AuNC substrate was evaluated experimentally and computationally to quantify its SERS enhancement and its suitability for use in a kinetic assay.

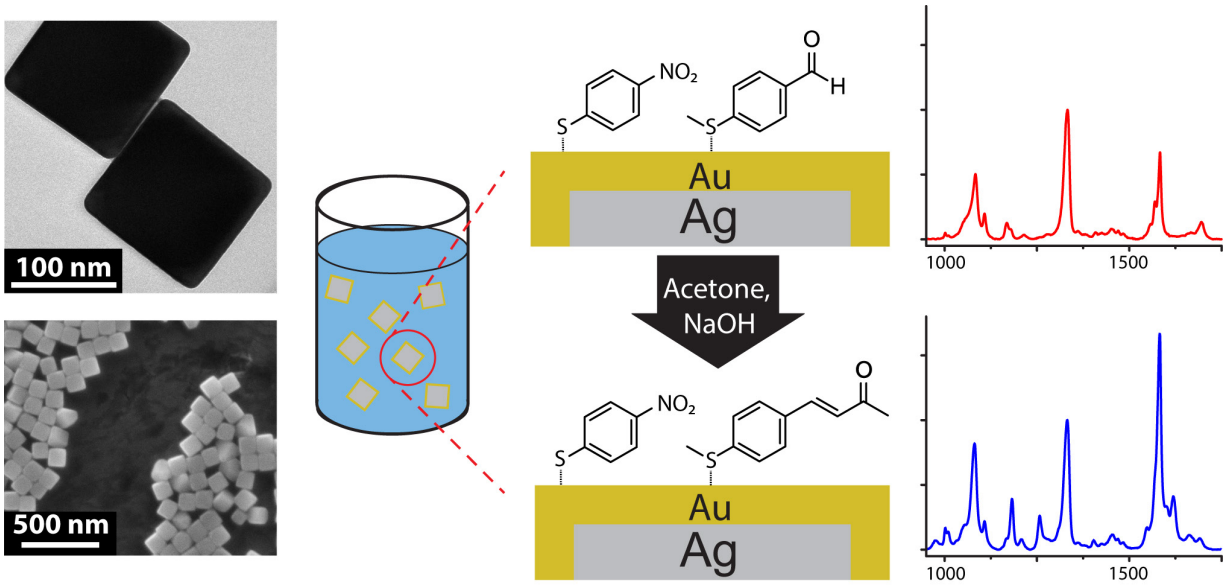

Figure 3. Schematic of the aldol condensation kinetic assay, with TEM and SEM images of the Ag@AuNC substrate.

In addition to the scaled-up synthesis of high quality SERS substrates, we introduced an internal standard – a reference molecule with high Raman activity that is bound to the substrate and whose SERS enhancement varies with time in the same manner as the target analyte. SERS spectra can be calibrated with respect to the spectral features of the IS, allowing the normalized

intensity of analyte peaks to serve as proxy for the relative concentration of analyte to IS. There are several schemes for the use of IS, including core-molecule-shell nanoparticle (CMS NP) systems[38-40] and simple surface adsorption systems. CMS NPs can be useful because the IS is protected from the surrounding environment, affording no opportunity for surface site replacement. However, the local dielectric environment of a shielded IS is not subject to exactly the same variations as that of the surface adsorbed analyte. The IS position inside the metallic substrate could result in diminished enhancement and their structure inhibits versatility – if a different IS molecule is desired, a new batch of CMS NPs must be synthesized. In contrast, surface-bound IS signal should correlate more closely with the analyte signal, and a single NP batch can be functionalized with any number of IS/analyte combinations. The potential for species desorption can be resolved by selecting an IS that covalently bonds to the surface. The IS/analyte co-functionalized Ag@AuNCs used as SERS probes in this work are capable of detailed quantitative analysis of reacting systems.

To demonstrate this quantitative analytical method, we report a kinetic study of the aldol condensation reaction of acetone and 4-(methylthio)benzaldehyde, using 4-nitrothiophenol as the IS; however, this is only a demonstration of platform capability. The method employed here can be easily modified for a quantitative examination of other reaction systems. Its highly sensitive nature allows probing of biological reactions and other highly dilute reactions. One must simply select a reactive species as the probe analyte, initiate a reaction by changing the probe media, and acquire spectral data over time. This simple, yet effective, method can yield a wealth of data and has good potential for practical applications.

Experimental and Computational Methods

Materials

1,5-Pentanediol 98% (PD) and 4-mercaptophenol 99% (MP) were purchased from Acros Organics. Silicone oil, polyvinylpyrrolidone avg. MW 55,000 (PVP), gold(III) chloride trihydrate 99.9% (chloroauric acid), and 4-(methylthio)benzaldehyde 95% (MTBH) were purchased from Sigma-Aldrich. Silver nitrate 99.9995% and sodium hydroxide pellets 98% were purchased from Alfa Aesar. L-Ascorbic acid 99.9% was purchased from Fisher Chemical. 4-Nitrothiophenol 98% (NTP) was purchased from Oakwood Chemical.

Silver–gold core–shell nanocube (Ag@AuNC) SERS probe synthesis procedure

The silver nanocube synthesis procedure was based on the polyol method.[41,42] Briefly, 20 mL of PD was heated with magnetic stirring in a silicone oil bath at 190 °C. When the PD reached approximately 130 °C, the reaction was initiated by injecting 250 μL silver nitrate solution (0.2 g, in 10 mL PD containing ~0.02 mg $CuCl_2$ seeding agent), immediately followed with 500 μL PVP solution (0.2 g, in 10 mL PD). Injections of 500 μL silver nitrate solution and 500 μL PVP solution were repeated every minute thereafter until the reactant solutions were consumed. The nanocube solution was washed repeatedly with 200 proof ethanol, purified by passing through a 0.22 μm filter, and suspended in a final volume of 50 mL ethanol.

The gold coating procedure was adapted from the protocol of Yang et al.[43] with few modifications. Briefly, 10 mL of AgNC solution were suspended into 10 mL ultrapure water and added to 1 L of PVP solution (1 mM, aqueous) under magnetic stirring, along with 250 mL ascorbic acid (10 mM, aqueous) and 50 mL NaOH (200 mM, aqueous). Next, a syringe pump (model NE-300, New Era Pump Systems, Inc.) was used to inject chloroauric acid (0.1 mM, aqueous) to the reaction mixture at a rate of 10 mL min^{-1}. When 200 mL chloroauric acid had

been added, injection was halted and the reaction was allowed to continue at room temperature for 10 minutes. The product, collected by centrifugation, was washed repeatedly with ultrapure water, filtered through a 0.22 μm filter, and stored in a final volume of 10 mL ethanol.

To make SERS probes from the nanoparticle substrate, the Ag@AuNCs were collected by centrifugation, suspended in an adsorbent solution containing the desired analytes, and incubated for more than 5 hours to ensure that the target molecules fully covered the NCs. The functionalized particles were then washed and suspended in clean solvent.

For the two-dye calibration experiments, the adsorbent solution was a mixture of NTP (20 mM, in ethanol) and MP (100 mM, in ethanol), blended in varying ratios, and the clean solvent was ultrapure water. To test the two-dye calibration's dependence on particle concentration, some of these samples were diluted with additional ultrapure water. For SERS enhancement factor quantification, the adsorbent solution was MP (160 mM, in ethanol) and the clean solvent was ethanol. For the aldol reaction experiments, a saturated ethanolic NTP solution was diluted 1:1000 with ethanol; the adsorbent solution was an equal volume mixture of this NTP solution and pure MTBH, and the clean solvent was ethanol.

Characterization of Ag@AuNCs

SEM images were obtained using a Quanta 600 FE-SEM (FEI Company, Hillsboro, OR) operated at 20 kV. This instrument was equipped with an Energy Dispersive X-ray spectroscopy (EDX) detector (Oxford Instruments, Abingdon, UK). TEM images were obtained with a Tecnai F20 FE-TEM (FEI Company) operated at 200 kV. EDX data was collected with this instrument using an EDX detector (Oxford Instruments) and an ultra-high resolution high-angle annular dark-field imaging (HAADF)- scanning transmission electron microscope (STEM) detector

(Fischione Instruments Inc., Export, PA). UV/Vis spectra were acquired with a FLUOstar Omega UV/Vis spectrophotometer (BMG Labtech, Germany).

Raman measurements were collected using a Thermo Scientific DXR Raman microscope (Thermo Fisher Scientific, Inc.) with 780 nm diode laser excitation, equipped with a Rayleigh rejection filter, a high resolution (~2 cm^{-1}) diffraction grating, and a CCD detector. Spectral intensity was acquired in the range of 300 cm^{-1}–1874 cm^{-1}. To measure, samples were loaded into a microwell plate (5 μL per sample), and the laser was focused just below the liquid surface by a 10× dark field objective. Each spectrum was acquired at 15 mW laser power with an integration time of 5 seconds and 4 accumulations.

Aldol condensation reaction

300 μL MTBH/NTP-coated Ag@AuNC was concentrated to a volume of 200 μL and combined with 50 μL acetone. To initiate the reaction, freshly prepared NaOH (1 M, in ethanol) was added to reach desired catalyst concentrations. Aliquots from the colloidal reaction mixture were drawn at various time points and used to obtain Raman and UV/Vis spectra. The reaction mixture was kept in a sealed vial to prevent evaporative loss of reagents, and it was vortexed and sonicated immediately before each aliquot was withdrawn. To ensure that spectral observations were indicative of aldol condensation reactions, a control experiment was also performed wherein the acetone was replaced by an equal volume of ethanol.

Spectral data analysis

To experimentally determine the SERS enhancement factor for MP, unprocessed bulk and SERS spectra were integrated in the 1559 cm^{-1}–1622 cm^{-1} region to obtain peak areas. The ratio of average SERS peak area to average bulk peak area was used for the calculation. For all other experiments, spectral data were first pre-processed in the Raman Processing software[44]

implemented in MATLAB 2013b (MathWorks, Inc., Natick, MA). This pre-processing performed baseline subtraction, noise reduction, and spectral normalization.

To obtain peak ratios for the co-functionalized MP/NTP Ag@AuNCs, the Peak Analyzer module in the OriginPro 9.1 software (OriginLab Corp., Northampton, MA) was used to fit Voigt peak profiles to the 1530 cm^{-1}–1630 cm^{-1} region. Peak height and area ratios were calculated from these fitted peaks; NTP:MP surface composition was approximated as the NTP:MP molar ratio in the probe adsorbent. Linear least-squares regression was used in OriginPro 9.1 to fit a line to the peak ratio vs. molar ratio data.

For quantitative kinetic analysis of the aldol reaction, each SERS spectrum was pre-processed as described above. For comparison, each raw spectrum was separately processed omitting the normalization step. The peak intensity at 1618 cm^{-1} was recorded for each processed spectrum. The intensity at $t = 0$ (approximated as the average intensity during the control run) was subtracted from each subsequent time point. This yielded the time-dependent relative intensity shifts that were used to fit a kinetic model. The model was a system of ordinary differential equations that represented stepwise elementary reactions simplified from the known mechanism of the aldol condensation reaction. The parameters in this model included four rate constants and the initial concentration of adsorbed MTBH. A scaling parameter was also introduced to convert spectral intensity to the concentration of product formed. The model solution was generated in MATLAB 2015a by the stiff ODE solver *ode23s*, using guess parameters and known initial conditions as inputs. The nonlinear model fitting function *fitnlm* was used to find the combination of parameter values that fit the model output to spectral data.

Simulation of electric field near nanocube surfaces

The electric field near a single nanocube was calculated by constructing a Finite Element Method (FEM) model in the COMSOL Multiphysics RF Module (AltaSim Technologies, Columbus, OH). The average geometric parameters of nanocubes observed through SEM and TEM imaging were model inputs, and the scattered electric field was the model output. The base model was a rounded cube of pure silver with edge length of 106 nm and with a 12 nm radius of curvature on edges and corners, surrounded by a sphere of solvent. The frequency-dependent bulk dielectric properties empirically determined by Johnson and Christy[45] were used to define silver and gold materials, and the solvent was defined by its frequency-dependent refractive index.[46,47] This model exhibits symmetry in the EM fields as well as the geometry, so the simulation space was truncated at the origin in the y and z planes, resulting in a quarter-sphere space. Excitation radiation was introduced as a monochromatic plane wave polarized along the z axis and traveling in the +x direction. The excitation wavelength was swept from 300 nm to 800 nm. To determine the effect of gold coating on the nanocubes, the simulation was repeated with a 1.5 nm layer of pure gold added to the cube surface.

Vibrational characterization

DFT calculations were performed in the Gaussian 09 software[48] in order to construct theoretical Raman spectra and assign vibrational modes to the spectra acquired during the aldol condensation reaction. Molecules involved in the condensation reaction were simulated, including NTP, MTBH, and 4-(4-methylthio)-3-buten-2-one. Optimized geometries and predicted Raman spectra can be found in Appendix A, along with details on the computational procedures.

Results and Discussion

Synthesis of Ag@AuNC SERS probe

Highly monodisperse AgNCs, prepared by the polyol method,[41] served as SERS substrates. In order to maintain the stability of the Raman sensors in harsh environments, the AgNCs were coated with a several atom thick layer of gold by adapting a published technique.[43] For this sensing application, large-scale synthesis of high quality sensors was critical. The AgNCs synthesis reached mass production (~100 mg); however, the published Au coating process was relatively small scale. We slightly modified the Au coating process (described in method section) to yield a larger batch of Ag@AuNCs (500 times scaled up). TEM and SEM images (Figure 3) demonstrated that the Ag@AuNCs maintain a cubic shape after Au film coating. The size of the nanoparticles was approximately 110 nm (Figure 4).

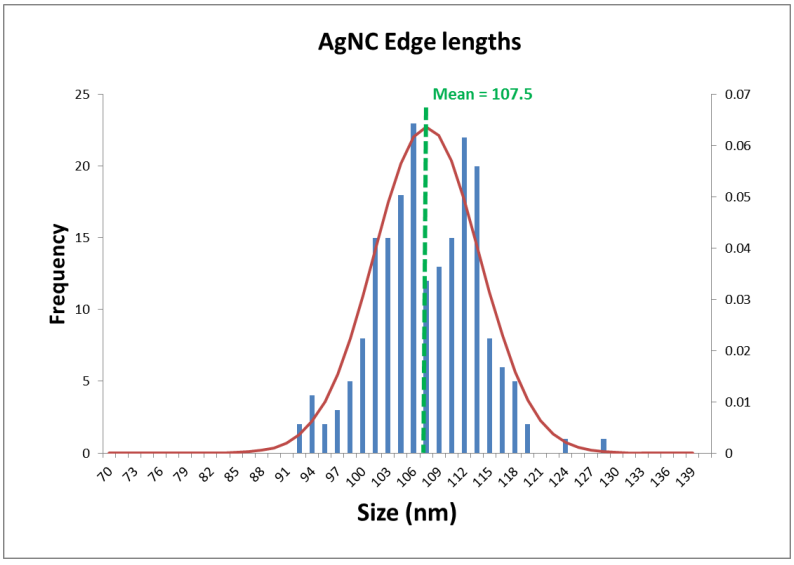

Figure 4. Size histogram of AgNCs used to make Ag@AuNC SERS substrate, overlaid with a fitted normal distribution.

EDX was used to confirm the Au film. Regions of the EDX spectral map acquired by SEM (Figure 5) that had a large number of nanocubes displayed a strong signal for silver and weaker signals for gold and carbon. The carbon signal could be from PVP, the capping agent on the surface of Ag@AuNCs. EDX maps acquired by HAADF-STEM clearly showed the localization of gold atoms on the surface of AgNCs (Figure 6).

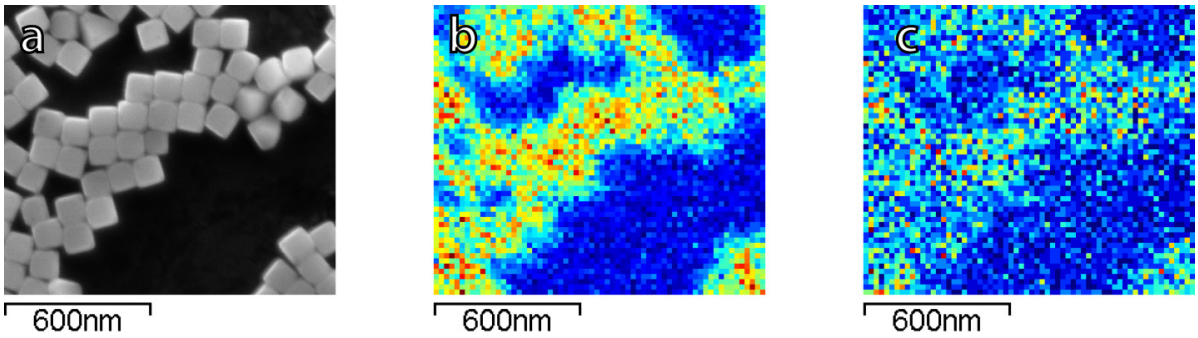

Figure 5. SEM image and EDX element maps for Ag@AuNCs. (b) and (c) are the element maps for Ag and Au, respectively.

To further demonstrate the presence of the Au film, Ag@AuNCs were sonicated in 10% aqueous HNO_3 for 2 hours and observed through TEM. The morphology of most Ag@AuNCs was unaffected. This result showed that the AgNC surfaces were successfully coated with a continuous layer of Au, and that this Au film provided adequate resistance to degradation from a strongly oxidizing solution. This assured that the Ag@AuNCs could withstand the milder conditions of subsequent sensing experiments for long periods of time without reducing their effectiveness as SERS substrates.

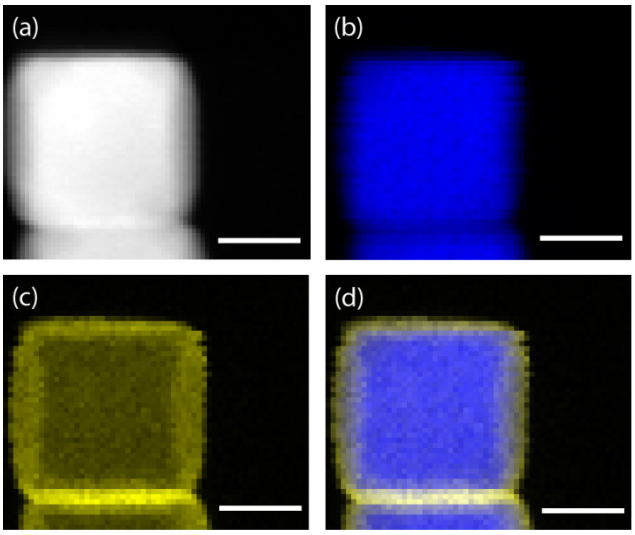

Figure 6. HAADF-STEM and EDX analysis of Ag@AuNC. (a) HAADF-STEM image; the EDX elemental maps of (b) Ag and (c) Au, respectively. Blue represents the intensity of the Ag L_α peak and yellow represents the average intensity of the Au L_α and Au M_α peaks; (d) combined elemental maps of Ag and Au. Scale bars are 50 nm.

SERS enhancement factor

The SERS enhancement factor, G_{SERS}, represents the fundamental figure of merit for SERS detection systems. It is defined as the ratio of the signal intensity per molecule of a SERS sample to the intensity per molecule of a bulk sample (eqn (1))

$$G_{SERS} = \frac{I_{SERS}/N_{SERS}}{I_{bulk}/N_{bulk}} \quad (1)$$

where I_{SERS} and I_{bulk} are the Raman intensities of a spectral peak for SERS and bulk samples, respectively. N_{SERS} and N_{bulk} are the number of molecules in the SERS and bulk samples that were sampled by the instrument during acquisition.

G_{SERS} was calculated experimentally for Ag@AuNCs by comparing the Raman intensity of the 1600 cm^{-1} peak for monolayer adsorbed MP with the intensity of an ethanolic MP solution. The excess MP was removed from the SERS sample, so N_{SERS} was calculated as the product of the nanocube concentration and the number of MP molecules on a single nanocube.

Nanocube concentration was estimated assuming 100% yield on nanocube synthesis and modification. The number of molecules per nanocube was estimated assuming maximum packing and an adsorption footprint area of 26 $Å^2$ for MP.[49,50] These assumptions overestimate N_{SERS}, which decreases the calculated value of G_{SERS}. This in turn means that our calculated SERS enhancement of $G_{SERS} = 3.88 \times 10^4$ is a conservative estimate.

Influence of Au film on SERS enhancement factor: simulation of electric field

To understand the influence of the Au film on the SERS enhancement factor, computational methods were employed to simulate the electric field environment of AgNCs and Ag@AuNCs. Because the protocols we adapted for Au coating were shown to deposit 3–6 atomic layers of gold, corresponding to a maximum Au film thickness of roughly 1.5 nm, this value was used for the Ag@AuNC simulation.

Simulation results were used to calculate the single particle UV/Vis extinction cross section as a function of radiation frequency, allowing the construction of predicted extinction spectra (Figure 7a). These calculated spectra predicted that the gold coating process should result in a redshift of the two main UV/Vis peaks as well as a change in their relative intensities. These calculated spectral shifts correlated closely with the experimentally obtained spectral shifts between the Ag@AuNC SERS probes and their AgNC precursors (Figure 7b). This similarity demonstrated that the computational model reasonably approximated the electric field environment of a single nanocube. Differences between calculated and observed spectra likely came from particle polydispersity and the ensemble of randomly oriented particles.

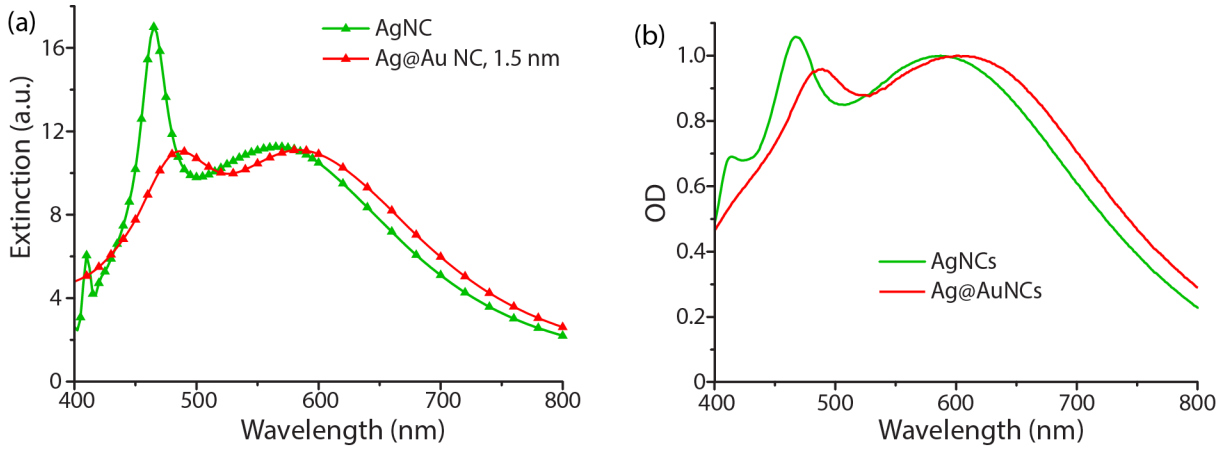

Figure 7. UV/Vis extinction spectra of AgNCs and Ag@AuNCs, determined (a) computationally and (b) experimentally.

To a first approximation, the enhancement of Raman signal due to electromagnetic effects, ${}^{EM}G_{SERS}$, is related the magnitude of the electric field as shown in eqn (2),[51]

$$ {}^{EM}G_{SERS} = \left|\frac{E_{loc}(\omega_i)}{E_0(\omega_i)}\right|^2 \left|\frac{E_{loc}(\omega_R)}{E_0(\omega_R)}\right|^2 \approx \left|\frac{E_{loc}(\omega_i)}{E_0(\omega_i)}\right|^4 \quad (2) $$

where E_0 is the electric field amplitude of the excitation, E_{loc} is the electric field amplitude at the location of the analyte, ω_i is the excitation frequency, and ω_R is the Raman shifted frequency. Because Raman frequency shifts are typically quite small, ${}^{EM}G_{SERS}$ is reasonably well approximated by the fourth power of the electric field's amplification at the particle surface. The computational model revealed the degree to which the nanoparticles amplified ambient electric fields. The magnitude of the electric field varied greatly across the surface of the nanocubes (Figure 8a). This pattern of localized amplification is itself a function of the radiation frequency, but for most frequencies in the simulation the field amplification remained concentrated around the corners and, to a lesser extent, the edges of the nanocubes. The electric field magnitude was calculated along the [111] vector for all simulated particle structures at an excitation wavelength of 780 nm (Figure 8b). Each structure showed a sharp increase in

$|E_{loc}|$ at the metal surface, followed by a rapid decay as the distance from the surface increased. The fields diminished to half their maximal value within ~12 nm of the surface. These results show that, for this excitation, the 1.5 nm gold coat on Ag@AuNCs does not noticeably alter either the maximum value or the decay length of $|E_{loc}|$.

The simulated electric field data at 780 nm excitation were used to calculate ${}^{EM}G_{SERS}$ for AgNC and Ag@AuNC. The maximal value of the electric field amplification near a single cube was 9.86 for Ag and 9.70 for Ag@Au. This corresponds to ${}^{EM}G_{SERS,Ag}$ = 0.95 × 10^4 and ${}^{EM}G_{SERS,Ag@Au}$= 0.89 × 10^4. The particle-averaged enhancement factor for the simulated Ag@AuNC was 470. This is lower than the experimentally determined value for our Ag@AuNC, but it is important to note that single particle simulations ignore any contribution from SERS hot spots. In many cases, a large proportion of SERS signal intensity originates from these hot spots;[52] therefore, it is likely that this computational enhancement factor underestimates the true value. This calculation also ignores SERS chemical enhancement, a phenomenon wherein the chemical bond with a metal surface increases the Raman cross section of some vibrational modes, which can further enhance SERS signal by a factor of ~10–100.[53] Chemical enhancement is a function of analyte geometry, surface composition, and the nature of the adsorption bond, and is difficult to independently quantify.[19] The exclusion of these effects from the model are most likely responsible for the disparity between the experimental and simulated SERS enhancement factors for Ag@AuNC. In summary, the comparable enhancements of Ag@AuNC and AgNC indicated that Ag@AuNC is a more optimal SERS substrate because of their resistance to harsh environments.

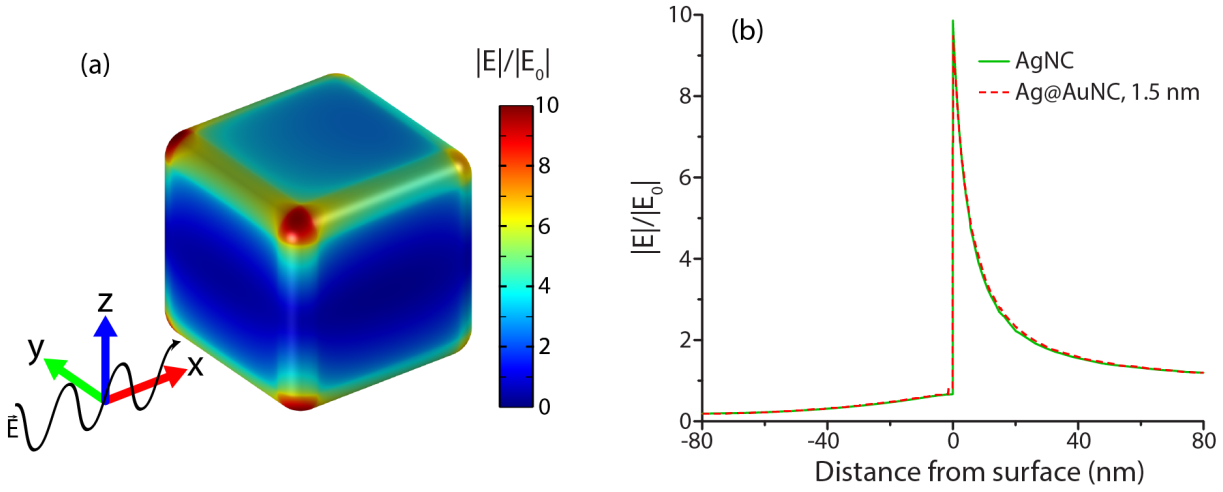

Figure 8. Calculated electric field enhancement on the surface of a single Ag@AuNC with a 1.5 nm Au coat, suspended in water. (a) Colormap rendering of electric field enhancement at particle surface; (b) calculated electric field enhancement for AgNC and Ag@AuNC, measured along a 111 vector that passes through the cube center.

Quantification through internal standard

Raman signal intensity is a linear function of the number of molecules sampled so, assuming constant excitation power and sampling volumes, intensity increases linearly with analyte concentration.[54] However, particle sedimentation and aggregation can drastically change the local concentration of adsorbed analyte within the sampling volume. Nanoparticle clusters can also alter the SERS enhancement factor as decreasing interparticle distance generates more SERS hot spots. In addition, volatile solvents and reactants are subject to evaporative loss under Raman excitation lasers, which changes the analyte concentration of the entire sample. All of these phenomena can introduce artificial changes in spectral intensity over time. Without calibration, the experimenter can not necessarily discern whether spectral shifts should be attributed to chemical reactions or to these confounding phenomena.

Our solution is to co-adsorb a nonreactive IS and use a characteristic spectral feature of that label species for spectral normalization. Spectral changes over time caused by changes in particle concentration or changes in SERS enhancement should be reflected equally in IS and

analyte species. Calibrating spectral intensity with respect to an invariant IS peak can ensure that any changes over time are the result of reactions. This analytical technique relies on the assumption that the relative spectral intensity of both species varies linearly with the relative amount of the adsorbed species, a restatement of the general dependence of Raman intensity on concentration. It also depends on the assumption that the spectra of multiple adsorbed species respond identically to changes in enhancement factor. If these assumptions hold, then there is no need to determine the number of nanoparticles in any given sampling volume – all that is needed to track kinetics is to measure the spectral evolution over time with respect to the immutable peak of the IS.

To verify these assumptions, we co-functionalized Ag@AuNCs with NTP and MP and performed SERS measurements while (1) varying the relative surface composition of the two analytes, and (2) varying the interparticle distance by particle dilution to alter the enhancement factor. Given the similarity in their chemical structures, we presumed that the relative surface composition of NTP and MP was approximately equal to their relative concentration in the adsorbent solution. Plotting the ratio of peak sizes against the ratio of adsorbate concentration [NTP]/[MP] yielded the expected linear trend (Figure 9a). To alter the amount of hot spot sampling, and therefore G_{SERS}, the particles were diluted to one half and one tenth of their original concentration. As the sample concentration decreased, the overall SERS intensity correspondingly diminished, resulting in weaker and noisier spectra. The resulting distributions of peak ratios for diluted and undiluted samples were compared. The results (Figure 9b) showed no significant difference in mean value at the $\alpha = 0.01$ level. While dilution did not significantly change the average peak ratio, it did increase the variance. Using the linear relation in Figure 9a, a 95% confidence interval about the sample mean for undiluted cubes resulted in a [NTP]/[MP]

prediction error of ±4.0% whereas the 95% confidence interval for one-half and one-tenth strength samples resulted in prediction errors of 6.4% and 8.2%, respectively.

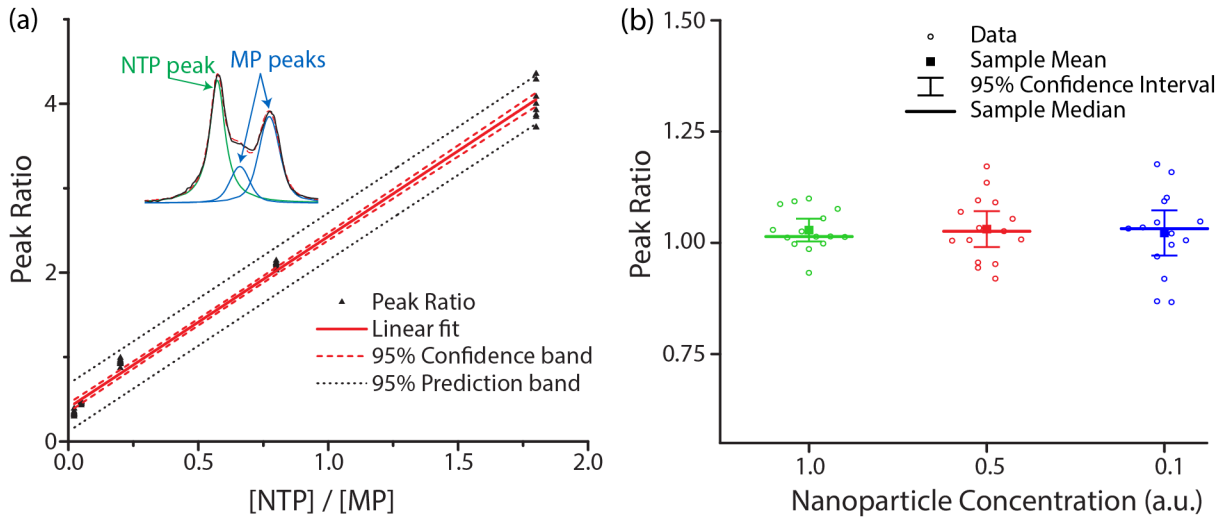

Figure 9. Analysis of peak ratio stability for 4-NTP and 4-MP. (a) Linear regression of peak ratios of the 1571 cm^{-1} and 1597 cm^{-1} peaks, as a function of the molar ratio NTP:MP in probe adsorbate. Inset: representative peak fitting; (b) scatter plot of peak ratios at various dilutions, including median, mean, and 95% confidence intervals.

Kinetic analysis of aldol condensation reaction

The IS co-adsorption method was used in conjunction with the Ag@AuNCs to quantitatively probe the reaction kinetics of the base-catalyzed crossed aldol condensation of surface adsorbed MTBH with free acetone. NTP was used as the IS. The aldol reaction mechanism was proposed by Nielsen and Houlihan (Figure 10).[55] First, the acetone is activated by base to its reactive enolate form in an equilibrium reaction step. The enolate then undergoes nucleophilic addition, forming a new C–C bond with the electrophilic carbonyl group of MTBH to form an aldol intermediate, 4-hydroxy-4-(4-methylthiophenyl)-2-butanone. Finally, water is eliminated via the E1cb mechanism, forming the α,β-unsaturated ketone product, 4-(4-methylthiophenyl)-3-buten-2-one. This elimination product is stabilized by conjugation with the

phenyl and carbonyl groups, and is the only product to form at high yield under the ambient conditions of this experiment.[56] The mechanism is summarized in eqn (3)-(5),

$$K + B \underset{k_2}{\overset{k_1}{\rightleftharpoons}} C + HB \tag{3}$$

$$C + A \overset{k_3}{\rightarrow} I + B \tag{4}$$

$$I + B \overset{k_4}{\rightarrow} P + B \tag{5}$$

where K is ketone (acetone), B is base, C is the carbanion of the acetone enolate, HB is the conjugate acid of the base, A is the aldehyde (MTBH), I is the intermediate aldol product, and P is the final α,β-unsaturated ketone product.

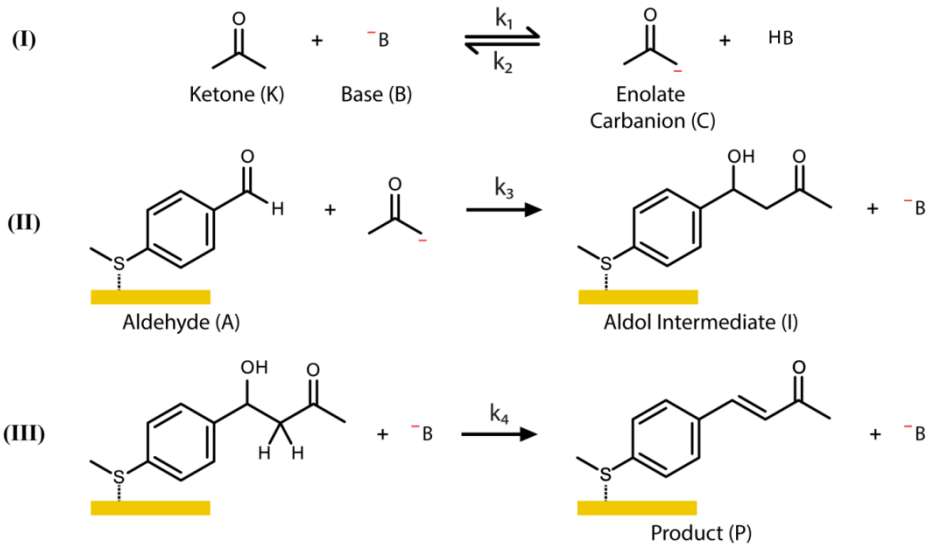

Figure 10. Reaction mechanism diagram for the aldol condensation of surface-adsorbed 4-(methylthio)benzaldehyde with free acetone.

The kinetic model (eqn (6)) proposed by Koudelka for the self-condensation of butanal[57] was modified to accommodate a crossed aldol reaction and to account for the additional

dehydration step that forms the observed product in this reaction.[58] [HB] was assumed to be constant in this model because it was the solvent and its fluctuations were small.

$$\frac{d}{dt}\begin{pmatrix}[K]\\[B]\\[C]\\[A]\\[I]\\[P]\end{pmatrix} = \begin{pmatrix}-k_1[K][B] + k_2[C][HB]\\ -k_1[K][B] + k_2[C][HB] + k_3[C][A]\\ k_1[K][B] - k_2[C][HB] - k_3[C][A]\\ -k_3[C][A]\\ k_3[C][A] - k_4[B][I]\\ k_4[B][I]\end{pmatrix} \quad (6)$$

MTBH was chosen because, lacking α-hydrogens, it cannot be activated by NaOH to perform self-addition and because its $–SCH_3$ group can bind to Ag@AuNC surfaces through thiol–gold interactions.[59] Furthermore, its electrophilic aldehyde carbon is much more susceptible to nucleophilic attack than that of a ketone.[55] This ensures that the acetone enolate will react with the cube-bound species preferentially; the side product formed by self-condensation of acetone should be minimal on the time scale of this experiment.[60] There is the possibility that NaOH could activate the terminal carbon of the product, resulting in the linkage of two MTBH molecules by a single acetone molecule. However, the acetone concentration in this experiment exceeds the MTBH concentration by a factor of $\sim 10^6$ so it is unlikely for unreacted MTBH to encounter the activated product molecule before reacting with an acetone enolate.

The aldol condensation reaction caused the extinction spectrum of the SERS probes to evolve with time (Figure 11). The OD increased and the main UV/Vis peak redshifted slightly with increasing reaction time, and a new feature appeared near 750 nm. These spectral alterations imply that the SERS enhancement factor for 780 nm excitation changes during the reaction.

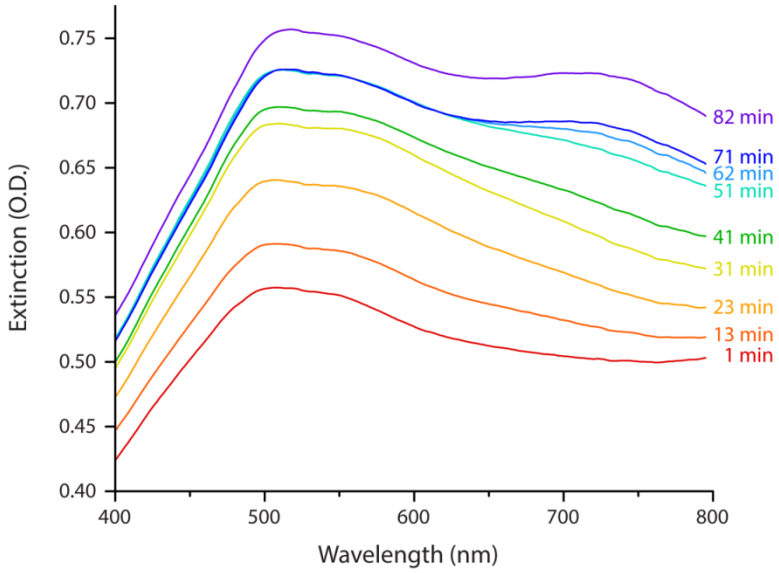

Figure 11. UV-Vis spectrum during aldol condensation reaction.

The reaction also caused the Raman spectrum of the SERS probes to evolve with time (Figure 12). The main peaks at the reaction start were at 1081 cm^{-1} (NTP, MTBH, product, $\nu C_{Aryl}–S$), 1110 cm^{-1} (NTP, $\nu C_{Aryl}–N$), 1340 cm^{-1} (NTP, νsNO_2), 1570 cm^{-1}, and 1580 cm^{-1} (phenyl quadrant stretch for NTP and MTBH, respectively). A weak peak existed at 1700 cm^{-1} due to the MTBH $\nu C=O$ vibration, and minor peaks from the ethanol solvent were also present at ~1050 and 1420–1500 cm^{-1}. Over the course of the reaction, notable features appeared at 1180, 1260, and 1618 cm^{-1}. These correspond to the condensation product and can be assigned to the phenyl in-plane C–H bending, the H–C=C–H rocking, and the $\nu C=C$ stretching, respectively. The peak at 1580 cm^{-1} increased dramatically in intensity as the reaction progressed because the Raman activity of the phenyl quadrant stretch is much higher for the condensation product than for MTBH (see Appendix A). Additionally, the aldehyde C=O stretch peak at 1695 cm^{-1} diminished over time and was undetectable by the reaction end.

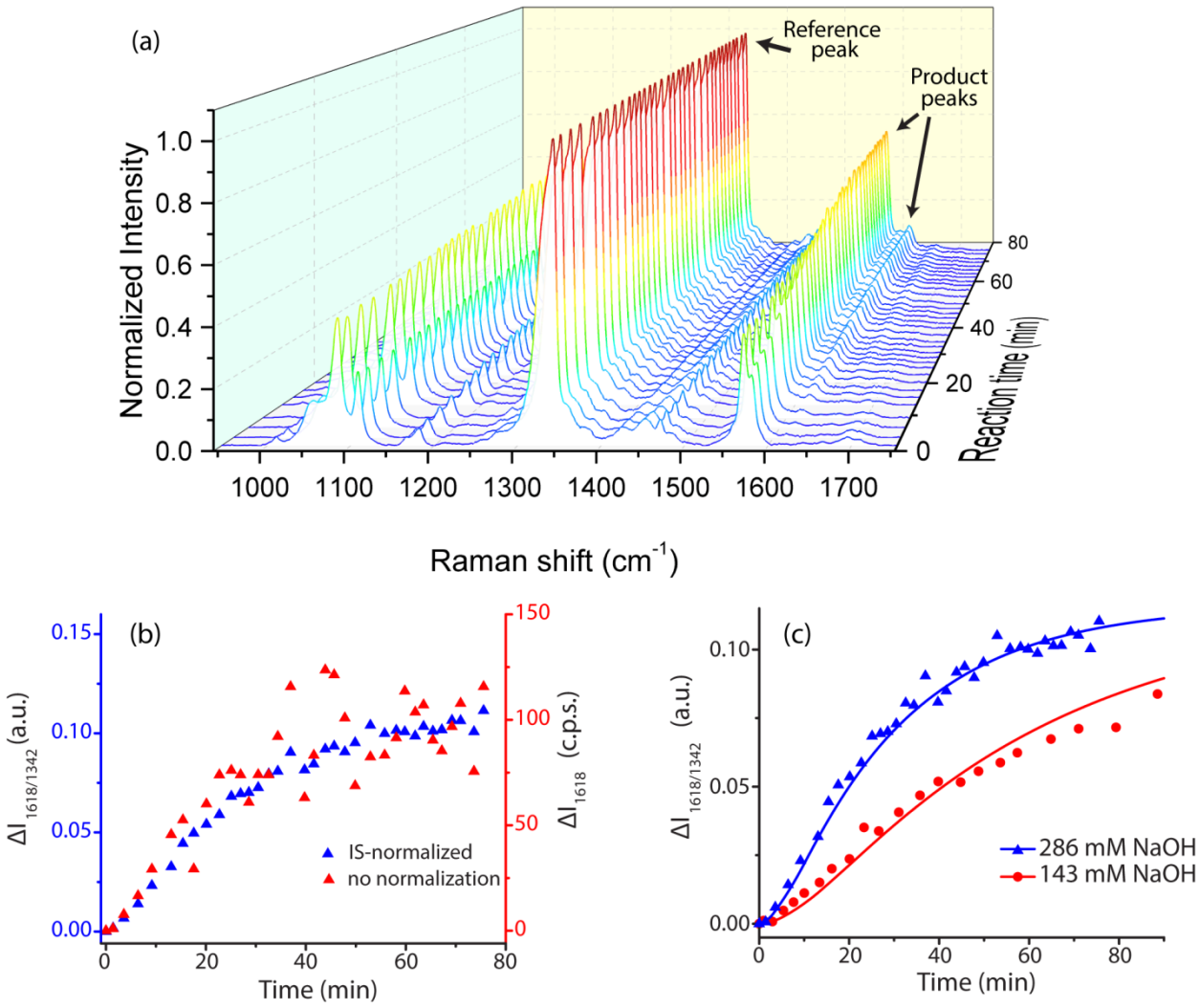

Figure 12. Results of the aldol condensation reaction between free acetone and adsorbed MTBH at room temperature, with adsorbed NTP present as the IS. Initial acetone concentration was 1.95 M. (a) 3D SERS spectrum showing time evolution during the reaction for the spectral range 950 cm^{-1}–1750 cm^{-1}. The initial NaOH concentration was 286 mM. (b) Intensity change over time of the 1618 cm^{-1} peak, comparing IS-normalized data (blue) to non-normalized data (red) at the same experimental conditions as (a). (c) The fitted kinetic model for 1618 cm^{-1} peak, using the parameters in Table 1.

The peak at 1618 cm^{-1} was used for quantification because it was distinct, appeared only in the final condensation product, and had sufficient signal to noise ratio. Plotting the IS-normalized intensities $I_{1618/1340}$ and the non-normalized intensities I_{1618} vs. reaction time clearly demonstrates that IS normalization greatly reduced the noise in the system (Figure 12b). This effectiveness implies that a large component of the noise in this system comes from variable

enhancement and variable analyte concentration within the sampling volume of the Raman laser. IS-normalized intensities were used in all subsequent analysis.

The fitted kinetic model predicted the values of the rate constants k_1, k_2, k_3, and k_4. Because the model is expressed in terms of concentration, an additional unit conversion parameter X was used to relate relative SERS intensity to relative sample concentration. NTP binds to Au surfaces with much greater strength than MTBH,[59] so it was not reasonable to assume that the molar ratio MTBH:NTP on Au surfaces was equal to that in the bulk adsorbing solution. Therefore, the initial concentration of adsorbed MTBH, $[A]_0$, was included as a model parameter. Parameter estimations, fitted to $I_{1618/1340}$, are tabulated in Table 1, and the fit is plotted in Figure 12c.

Table 1. Kinetic Parameters for Aldol Condensation Reaction

Parameter	Fitted Value (± std. error)	Reference[57]
k_1 (M^{-1} min^{-1})	4.796 ± 2.04	4.163
k_2 (M^{-1} min^{-1})	0.0060 ± 0.0036	0.0015
k_3 (M^{-1} min^{-1})	0.1197 ± 0.0036	4.686
k_4 (M^{-1} min^{-1})	129.206 ± 55.01	N/A
$[A]_0$ (μM)	7.916 ± 0.220	N/A
X (μM^{-1})	0.0148 ± 0.0005	N/A

Based on estimated nanocube yields and dilution factors, the predicted value of $[A]_0$ was physically realistic, corresponding to a surface monolayer composed of approximately 9.7% MTBH and 91.3% NTP by number. The values of the rate constants k_1 and k_2 were in reasonable agreement with the published values for the self-condensation of butanal.[57] Our observed k_3 was significantly lower than that for self-condensation of butanal; this could be explained by a lower reactivity for MTBH due to its resonance stabilization and its bulkier structure, or by the steric hindrance of the surface monolayer in our experiment.

Chapter Conclusion

In conclusion, we have achieved the large-scale synthesis of high quality Ag@AuNCs and characterized them for use in colloidal suspensions as a SERS substrate. The Ag@AuNCs demonstrated SERS enhancement and good stability in varied environments. The enhancement factor was calculated both experimentally and computationally. We demonstrated, by investigating the kinetics of an aldol condensation reaction at dilute reagent concentrations, that an internal standard can be co-functionalized on our substrate to yield a SERS probe capable of highly sensitive analyte quantification. This probe is versatile, enabling the use of many combinations of IS and analyte including combinations with different adsorption behaviors, provided both species can adsorb to probe surfaces. The IS correction adequately accounts for aggregation and other phenomena which affect the SERS enhancement factor, rendering this probe suitable for kinetic assays in diverse conditions, including reactions with highly dilute reagents and reactions in complex media or harsh environments. Furthermore, our analyte/IS functionalized Ag@AuNC probe has great potential in the biological and biomedical fields, and our current investigations center on extending their use for these applications.

CHAPTER III

LOW-COST AND SIMPLE FABRICATION OF NANOPLASMONIC PAPER FOR COUPLED CHROMATOGRAPHY SEPARATION AND SURFACE ENHANCED RAMAN DETECTION*

Chapter Summary

Surface-enhanced Raman scattering (SERS) is a powerful analytical tool which enables the detection and identification of analytes adsorbed on nanostructured noble metals. However, SERS analysis of complex mixtures can be challenging due to spectral overlap and interference. This chapter demonstrates a method to simplify the identification of mixed-analyte samples by coupling SERS detection with chromatographic separation on a nanoplasmonic paper substrate. This "nanopaper" substrate is a silver coated glass microfiber filter paper which possesses large SERS enhancement and can serve as a stationary phase in paper chromatography. Nanopaper is easily synthesized using the silver mirror reaction, making it a highly accessible technology. Nanopaper was successfully used as a combined paper chromatography-SERS (PC-SERS) substrate in the separation and identification of mixed organic dyes. It was further employed to separate and identify lycopene and β-carotene in commercial food products, demonstrating the versatility and utility of nanopaper in the identification of complex mixtures.[61]

---

* Reproduced with permission from Weatherston, J. D., Seguban, R. K. O., Hunt, D. & Wu, H.-J. Low-Cost and Simple Fabrication of Nanoplasmonic Paper for Coupled Chromatography Separation and Surface Enhanced Raman Detection. *ACS Sensors* 3, 852-857, doi:10.1021/acssensors.8b00098 (2018).

Introduction

Raman spectroscopy is a valuable detection tool because of its fingerprint identification of molecules, allowing for multiplexed analyte detection. Surface-enhanced Raman scattering (SERS) offers an improvement over normal Raman by increasing signal strength to allow detection of extremely dilute species. Furthermore, the advent of portable Raman spectrometers enables SERS for on-site work in diverse disciplines such as law enforcement forensics, environmental quality testing, food and drug testing, and point-of-care medical testing.[62-65]

SERS is a near-field effect which greatly enhances the Raman scattering signal near nanostructured metal surfaces, primarily due to the localized electric field enhancement at such interfaces.[66] The degree of enhancement is highly dependent on substrate composition and morphology; thus, the design of the SERS substrate is central to obtaining good results. Diverse classes of SERS substrates have been developed for sensing applications, including nanoparticle sols, chemically roughened metal surfaces, and solid supports modified with metal films.[40,67,68] However, the fabrication of reported SERS substrates is often tedious and relatively costly, which limits the accessibility of SERS substrates.

Another challenge in SERS identification is common across spectroscopic methods: interpretation of spectral data. Depending on the sample, spectral interpretation can range from straightforward to highly challenging. As the number of chemical species in a sample increases, SERS peaks are more likely to overlap, confounding features. Peak fitting procedures can help resolve overlapping signals, but such treatments are often highly sensitive to user input. More sophisticated statistical methods, such as principal component analysis or hierarchical cluster analysis, may also be used to resolve a complex spectrum into its contributing component spectra.[69-71] These methods are useful, but require large data sets and reference libraries to be

successful.[29] A different approach to simplifying spectral data is to couple spectral analysis with a pre-separation procedure. This strategy enables collection of multiple simple spectra rather than a single complex spectrum in a process analogous to other common separate-and-then-detect methods like liquid chromatography–mass spectrometry (LC–MS). The combination of separation with molecular detection is a synergistic one. The separation process alone differentiates analytes but usually cannot uniquely identify them. In contrast, SERS spectra contain the information necessary for molecular identification, but can be challenging to interpret for mixed analytes.[72] Prior studies have successfully coupled SERS with various separation methods, such as liquid chromatography (LC-SERS), thin layer chromatography (TLC-SERS), and Western blot, resulting in improved sensing performance.[73-77] However, these methods require specialized instrumentation and would be difficult to perform in a nonlaboratory setting.

A simpler and more accessible choice for separation is paper chromatography (PC), which is a well-established method for the separation of biological analytes. In PC, analytes are deposited on a paper or paper-like substrate and a mobile phase is eluted through the substrate via capillary action. Separation occurs based on phase partitioning (i.e., solubility in the mobile phase) and affinity (i.e., interaction between analyte and substrate).[78] While other chromatographic methods can result in superior separation, the simplicity and accessibility of PC nevertheless make it a useful tool.[78] Achieving PC-SERS requires a substrate that functions as a PC stationary phase while also providing Raman enhancement for SERS identification. Previous studies have synthesized PC-SERS substrates by modifying porous solid surfaces with noble metals using various methods, including inkjet printing nanoparticle ink onto cellulose paper,[29] thermally evaporating and annealing silver films on cellulose paper,[79] impregnating chromatography paper with silver–silica core–shell nanoparticles,[80] and modifying glass fiber

sheets with molybdenum disulfide followed by reduction of chloroauric acid.[81] These PC-SERS substrates were successfully used to separate and detect various substances such as organic dyes and narcotic drugs; however, each required multiple complicated synthetic steps to produce, limiting accessibility for widespread use.

In this study, we utilized the silver mirror reaction with commercial glass microfiber filter paper in a facile protocol to synthesize nanoplasmonic paper (called nanopaper). Nanopaper is a glass microfiber filter paper decorated with a dense layer of silver nanoparticles, which possesses large SERS enhancement. The well-known mirror reaction offers a rapid, simple, robust and effective way to form silver deposits on a large amount of glass fiber papers in a single batch reactor.[82] The granular nanostructured silver film can be created by controlling the reaction conditions, offering large SERS enhancement to silica substrates.[82-84] Nanopaper proved to be a viable PC-SERS substrate capable of the separation and identification of mixed organic dyes. Furthermore, the facile, scalable synthesis requires very few materials and little expertise, allowing this separation-detection technology to have broad accessibility across multiple research disciplines. In order to demonstrate the versatility of nanopaper, we further utilized it to analyze the carotenoid profile in commercially available food products, including carrot and tomato juices and vegetable juice blend.

Experimental Methods

Materials

Potassium hydroxide pellets, ammonium hydroxide solution (28–30%), rhodamine 6G (95%), crystal violet (90%), toluene (99.5%), dichloromethane (99.5%), anhydrous magnesium sulfate, and lycopene (90%, from tomato) were purchased from Sigma-Aldrich. β-Carotene (97%) was acquired from Enzo Life Sciences. Acetone (99.8%), hexanes (99.9%), 2-propanol

(99.9%), methanol (99.9%), acetic acid (glacial), silver nitrate (99.9995%), and Whatman™ binder-free glass microfiber filters (grade 934-AH, 110 mm circles) were purchased from Fisher Scientific. d-Glucose (99.5%), methyl orange (ACS grade), ethanol (200 proof), and cresol red (pure, indicator grade) were purchased from VWR International. Before use, the lycopene solid was rinsed with methanol and allowed to dry. All other materials were used directly without further purification. Carrot juice (Bolthouse Juice Products LLC), tomato juice (Campbell Soup Company), and V8 Original juice blend (Campbell Soup Company) were purchased from a local market.

Nanopaper synthesis

Nanopaper PC-SERS substrate was synthesized by performing the silver mirror reaction in the presence of glass microfiber filters. Tollens' reagent was prepared according to a reported protocol[85] by adding potassium hydroxide (3.2% aqueous) to 40 mL of 2% silver nitrate solution until a brown precipitate formed, followed by dropwise addition of ammonium hydroxide (~30%) until the solution became colorless and transparent. Additional silver nitrate was added until a yellow color persisted, and finally diluted ammonium hydroxide (6%) was added until the solution again became transparent. Immediately after its preparation, a stack of four glass microfiber filters was immersed in the Tollens' reagent solution. To initiate the mirror reaction, 40 mL of 35% aqueous d-glucose solution was combined with 20 mL methanol and then added to the Tollens' reagent, shaking to mix thoroughly. The glass microfiber filters were left in this reaction mixture for 1 h, then removed and washed with copious amounts of water and 2-propanol. The resulting nanopaper was stored immersed in 2-propanol, protected from light.

Carotenoid extraction from vegetable juices

To extract carotenoids from the vegetable juices (carrot juice, tomato juice, and V8 Original juice blend), we adapted a reported protocol.[86] Briefly, 5 mL of juice was added to 5 mL of 1:1 hexane:acetone (v/v). The mixture was vortexed and sonicated, then centrifuged. The organic phase was then saponified with potassium hydroxide solution (40%, in methanol) at 56 °C for 45 min. The extract was then washed with 10% aqueous magnesium sulfate, filtered to remove solids, washed 3 times with water, dehydrated over anhydrous magnesium sulfate, and filtered. This left an extract containing water-insoluble, nonsaponifiable organics, including carotenoids. The extract was concentrated in a rotary evaporator, reconstituted in a minimal volume of dichloromethane, and stored at –20 °C, protected from light.

PC-SERS with nanopaper

Nanopaper samples were removed from storage, cut into strips, and air-dried. To prepare a nanopaper strip for PC, ~0.25 μL of analyte solution was spotted by micropipette near the bottom edge and allowed to dry. Then, the sample was loaded into a beaker containing the mobile phase, taking care to avoid direct contact between the mobile phase and the analyte spot. The mobile phase used for the 4-dye mixture was 9:1 (v/v) toluene/acetic acid, and the mobile phase used for carotenoid separation was absolute ethanol. When the solvent had migrated a sufficient distance up the nanopaper, the paper was removed, the location of the solvent front was marked, and the sample was oven dried before SERS data collection.

Raman measurements were collected using a Thermo Scientific DXR Raman microscope (Thermo Fisher Scientific, Inc.) equipped with 780 nm diode laser excitation, a 10x objective lens, a Rayleigh rejection filter, a high-resolution (~2 cm^{-1}) diffraction grating, and a CCD detector. Spectral intensity was acquired in the range of 400 cm^{-1}–1800 cm^{-1}. Each spectrum was

acquired at 1 mW laser power with 5 accumulations of 1 s integration time. Developed chromatograms were measured at regular intervals (0.25 mm for 4-dye mixture, β-carotene, and lycopene, and 0.50 mm for juice extracts) on a line parallel to solvent flow to construct SERS maps. The Omnic software package was used to smooth and baseline correct spectra; all spectra were then scaled with respect to the nanopaper background signal at 900 cm^{-1} to account for sample roughness, which caused small variations in overall spectral intensity as the sample surface deviated above or below the microscope focal plane. To construct component intensity profiles from the processed SERS maps, scaled intensity was determined for characteristic wavenumbers and averaged to achieve 1 mm spatial resolution. Each intensity profile relates the results of a single PC-SERS experiment.

Results and Discussion

Nanopaper synthesis and characterization

The nanoplasmonic PC-SERS substrate, which we call "nanopaper", was designed with three criteria in mind: (1) it should be easily synthesized from readily available materials; (2) it should facilitate the separation of compounds based on their physical properties; and (3) it should possess sufficient SERS enhancement to allow detection of analytes that would otherwise be difficult to identify. These criteria are essential to the utility and accessibility of the nanopaper product.

Nanopaper was synthesized by modifying binder-free glass microfiber filters. The glass filters serve as a mechanically strong support that is relatively chemically inert. Their structure of intertwined glass fibers is also conducive to capillary action, which drives mobile phase elution in paper chromatography. Because glass does not provide the SERS enhancement necessary to a PC-SERS substrate, the mirror reaction was employed to impregnate the glass fiber filters with

silver, the element with the largest SERS enhancement. In this simple and straightforward reaction, glucose was used to reduce diamine silver(I), resulting in elemental silver particles which precipitated on the glass fiber surfaces. The silver mirror reaction was chosen for its simplicity and familiarity, as well as its effectiveness in coating glass surfaces with silver. All synthetic steps, including reagent preparation, reaction, and purification, could be completed in a large batch reactor in less than 2 h.

Nanopaper synthesis results were analyzed by visual appearance, SEM, and SERS. During synthesis, the color of the glass microfiber filters changed from white to dark gray/brown, indicating the deposition of silver particles (Figure 13c). This was confirmed by SEM, which showed a dense layer of nanoparticles covering the glass fiber surfaces (Figure 13a), with average particle size below 100 nm, and an average nearest-particle distance less than 20 nm in most samples (Figure 14, Figure 15). The morphology of the silver coating was not observed to change after performing paper chromatography.

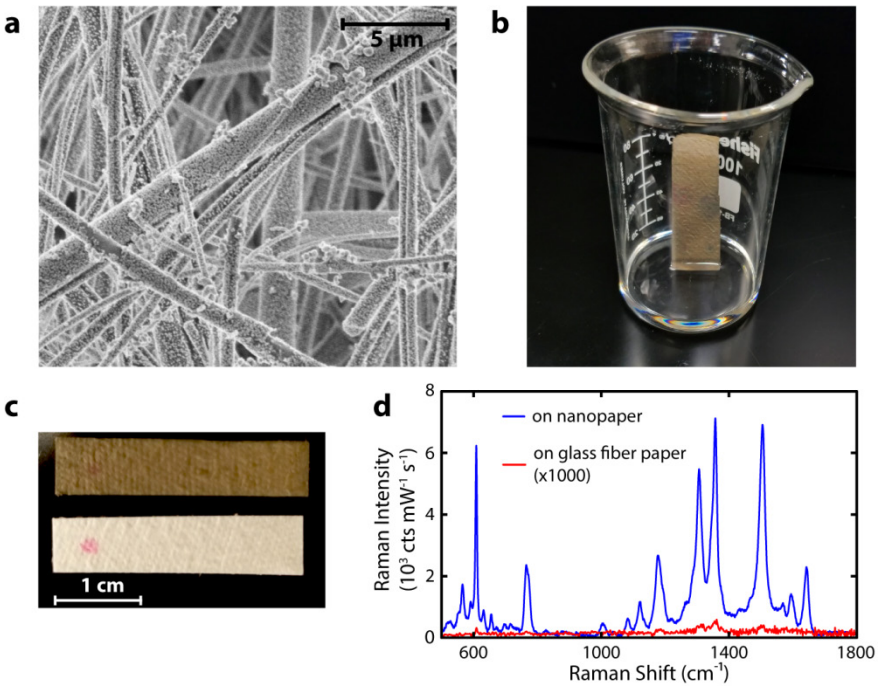

Figure 13. Results of nanopaper synthesis. (a) SEM micrograph of nanopaper. (b) Photograph illustrating PC on nanopaper substrate. (c) Photograph comparing nanopaper (top) with its glass microfiber filter precursor (bottom); each was spotted with R6G near the left edge. (d) Raman signal comparison of 10^{-4} M R6G adsorbed on nanopaper (blue) and 4×10^{-4} M R6G adsorbed on glass microfiber filter (red, scaled by 1000 times for visibility).

The SERS activity of the nanopaper was determined by comparing the Raman signal of rhodamine 6G (R6G) adsorbed on unmodified glass fibers against the SERS signal of R6G adsorbed on nanopaper (Figure 13d). The result showed large signal from the nanopaper sample while the plain glass fiber sample could barely be detected, indicating that the silver coating of the nanopaper provided SERS enhancement. The analytical enhancement factor[54] was approximated by calculating the peak intensity ratio of the SERS and normal Raman samples. For the 612 cm^{-1} peak of R6G, the enhancement factor was 1.15×10^5 (Figure 13). To further verify nanopaper reproducibility, the enhancement factor was calculated for three different batches of nanopaper, synthesized on different days, using a different dye solution (0.4 mM crystal violet). For the 417 cm^{-1} peak of CV, effective enhancement factors of the three different

batches were 1.15×10^5, 1.17×10^5, and 1.05×10^5. The consistent enhancement between nanopaper batches demonstrated the reproducibility of the nanopaper synthesis procedure.

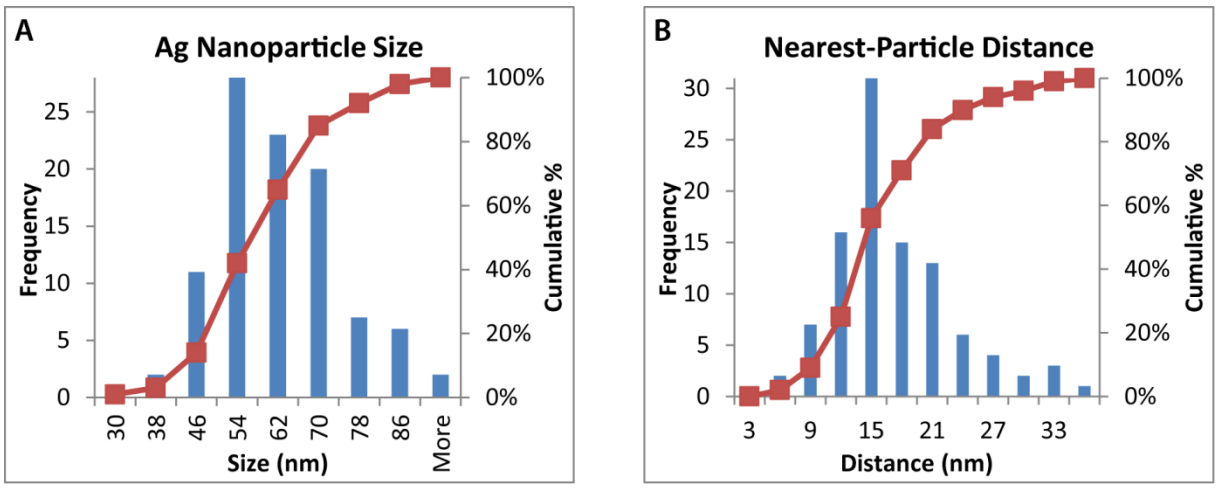

Figure 14. Characterization of silver nanoparticles found on nanopaper. Size (a) and spacing (b) distributions of silver nanoparticles on nanopaper, based on SEM micrographs. 100 distinguishable particles were chosen and their diameters were measured, along with the distance to the nearest distinguishable particle.

Overall, the nanopaper exhibited good durability throughout experiments. Changes in physical properties and SERS activity were not observed during the various drying, elution, and SERS measurement steps of the PC-SERS protocol, or after brief periods of oven drying (<1 h at 75 °C). After extended time (>1 day) on the benchtop or in the oven, nanopaper lost some SERS activity, became hydrophobic, and experienced a slight change in color (Figure 16); thus, all SERS measurements of nanopaper samples were performed within the same day the sample was removed from storage. However, when stored in isopropanol and protected from light and air, we observed no noticeable degradation of the nanopaper over a period exceeding 2 months.

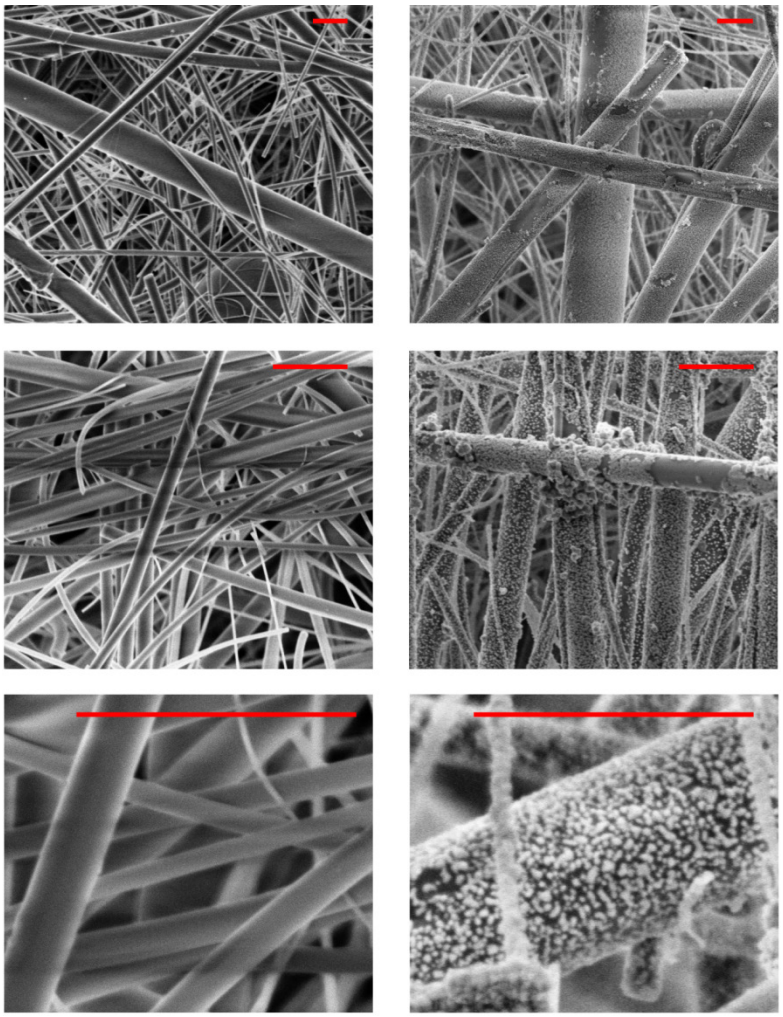

Figure 15. SEM comparison of glass fibers before (left column) and after (right column) the silver mirror reaction. All scale bars are 3 μm.

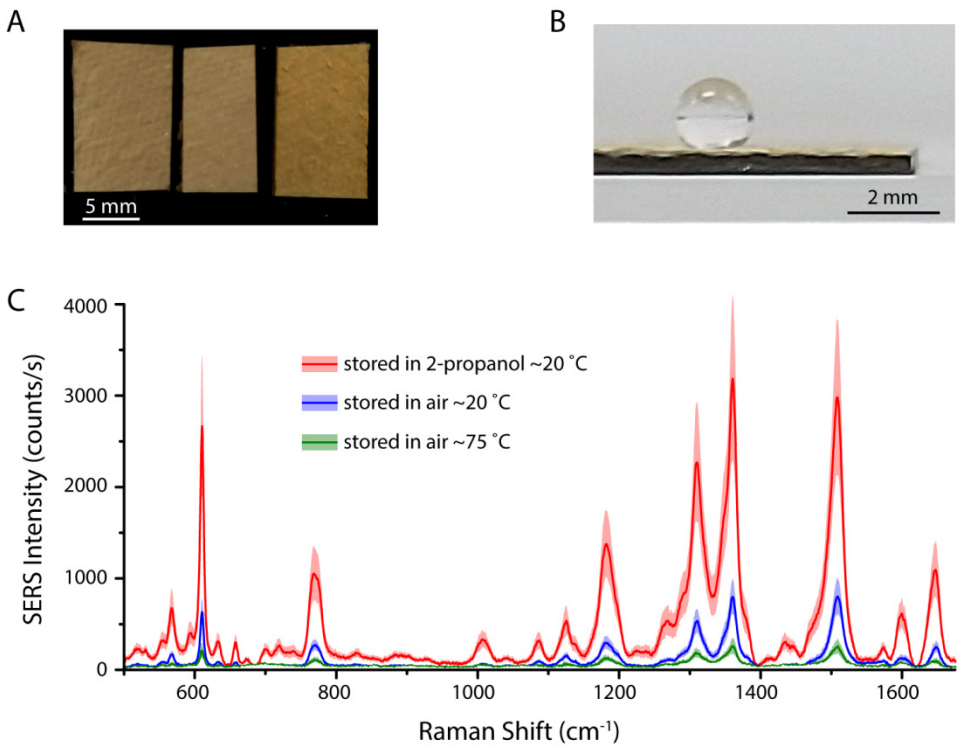

Figure 16. Comparison of nanopaper storage conditions. (A) Photograph of nanopaper samples stored under 2-propanol (left), in air at room temperature (center), and in an oven at 75 °C (right) for 2 days. (B) 3 µL water applied to oven-stored nanopaper, showing hydrophobic character. Water deposited on room temperature samples was absorbed by the nanopaper. Significant lateral spreading of the water was observed on the sample stored under 2-propanol, but with virtually no spreading was observed on the air-stored sample. (C) SERS comparison of R6G applied to nanopaper samples in (A). Spectra were acquired at 5 random spots for each sample. Curves show the mean spectra and shaded regions are standard deviations.

PC-SERS performance

PC-SERS performance Nanopaper performance was tested by implementing the PC-SERS protocol on a mixture of four organic dyes: R6G, cresol red (CR), crystal violet (CV), and methyl orange (MO) (see Figure 17 for dye structures). The dye mixture (4×10^{-4} M in each dye, aqueous) was spotted on nanopaper and eluted with a mobile phase of 9:1 (v/v) toluene:acetic acid. During elution, dye spots were observed to migrate upward, separating into three faintly colored bands. These bands faded upon drying the nanopaper, becoming invisible or barely visible and making the developed chromatogram challenging to interpret visually (Figure 17).

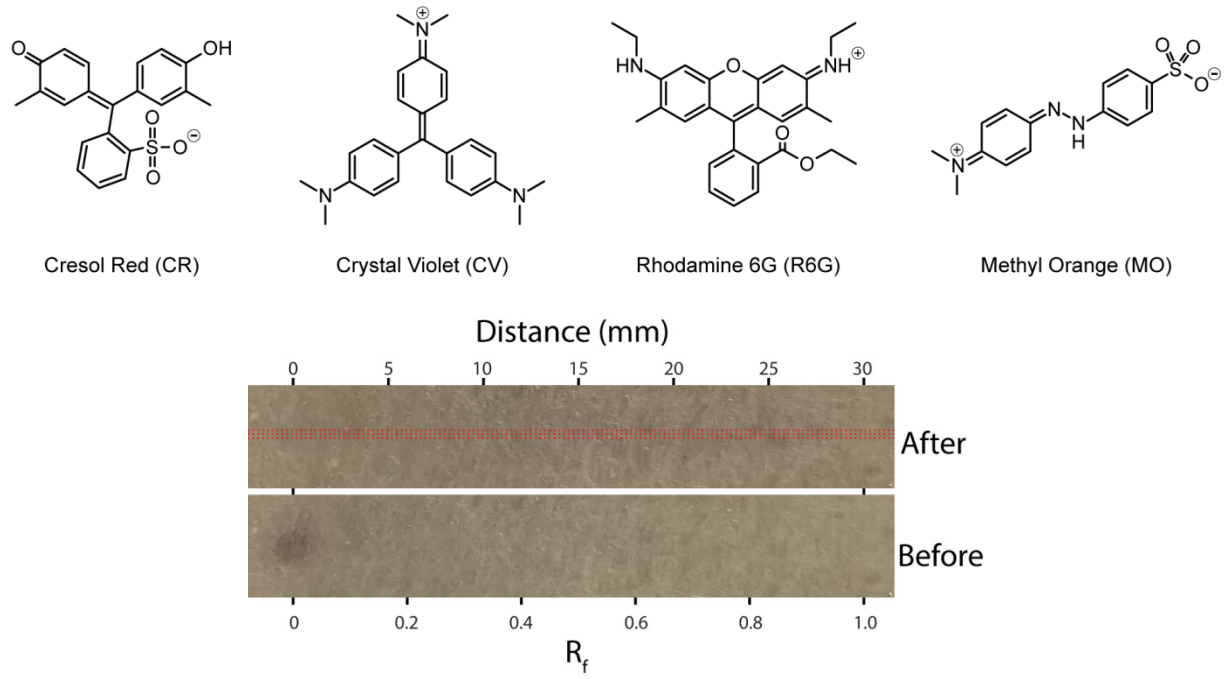

Figure 17. Visual results of PC on a mixture of 4 organic dyes. Top: molecular structure of the 4 organic dyes used in PC-SERS performance test, at pH ~2.5. Bottom: Photographs of PC-SERS nanopaper chromatogram before and after the PC separation of 4 organic dyes. The grid of SERS measurement locations is overlaid in red.

The SERS mapping results helped to interpret the PC separation, showing distinctly different spectral patterns across the length of the chromatogram (see Appendix B for spectral results). The location of each dye was determined based on the SERS intensity profile of its characteristic peak (Figure 18), and expressed in terms of a retardation factor (R_f). R_f is the fractional migration distance from the initial spot relative to the total migration distance of the mobile phase, and is calculated as shown in eqn (7),

$$R_f = \frac{x_i - x_0}{x_{front} - x_0} \tag{7}$$

where x_i, x_0, and x_{front} are the locations of the ith measurement, the center of the initial spot, and the solvent front, respectively. The intensity profiles identified the composition of the three bands observed during PC: the first band contained CR with a maximum intensity at $R_f \approx 0.11$,

the middle band contained MO with a maximum intensity at $R_f \approx 0.30$, and the third band contained both CV and R6G with maximum intensities at $R_f \approx 0.84$ and $R_f \approx 0.87$, respectively. The primary factor in elution distance appears to be solubility in the mobile phase used, based on our observation that the dyes eluted in the order of increasing solubility in 9:1 toluene:acetic acid (CR < MO < CV/R6G).

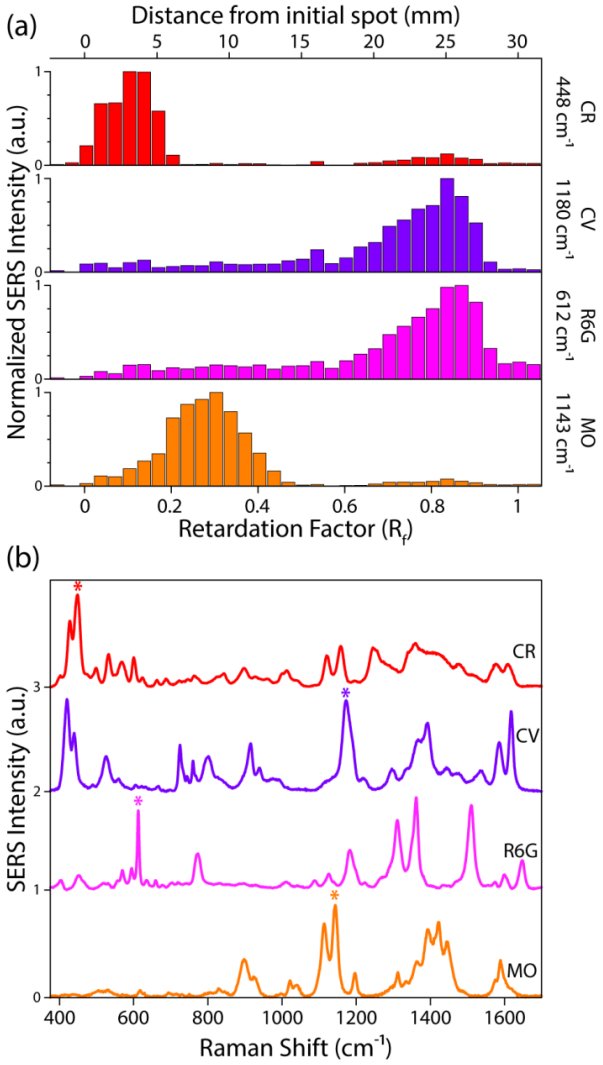

Figure 18. Spectral results of PC-SERS on a four dye mixture. (a) Intensity profile of the characteristic peak for each dye, as a function of R_f (lower axis) and migration distance (upper axis). Each profile is normalized by its own minimum and maximum values to clearly show species localization. (b) Reference SERS spectra of the four dyes (scaled and shifted for clarity). Peaks used to construct species profiles are denoted *.

The separation resolution of this PC-SERS result was not as good as some other chromatographic techniques, such as TLC and LC. Co-elution of CV and R6G occurred, and some band spreading, or streaking, was present for all species. We believe this could be improved by functionalizing the surface to modify hydrophobicity or by selecting a better mobile phase. However, the separation was sufficient to easily distinguish spectral constituents by SERS, making such optimization superfluous in this case.

PC-SERS demonstration with extracted carotenoids

To further demonstrate the utility of PC-SERS with nanopaper, we applied the technique to identify β-carotene and lycopene in food products, including tomato juice, carrot juice, and V8 original juice blend. β-carotene (highly enriched in carrot) and lycopene (mainly found in tomato) are two major carotenoids that can serve as precursors of retinol and bioactive antioxidant compounds, playing an important role in human health.[87] Due to the chemical similarity of β-carotene and lycopene, traditional analyses of carotenoids combine high-performance liquid chromatography (HPLC) with different detection methods (e.g., UV/vis or mass spectrometers) to improve specificity.[88] The requirement of special instruments limits the accessibility of carotenoids analysis; thus, our nanopaper technique offers an alternative solution for food industry.

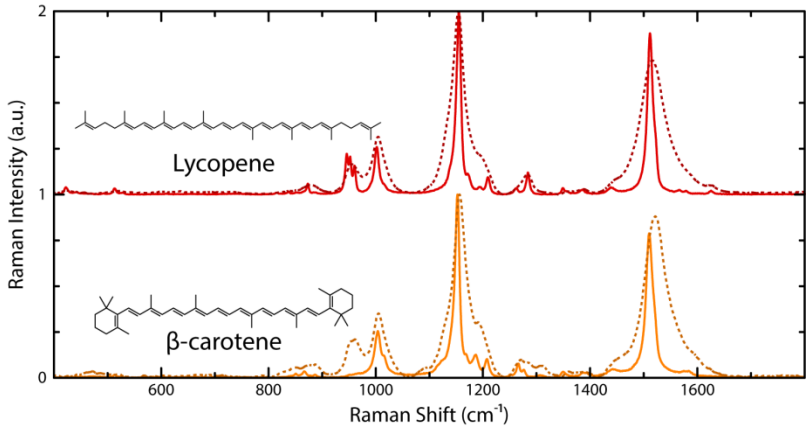

Figure 19. Spectral comparison of solid phase (solid line) and SERS (dashed line) spectra for reference lycopene and β-carotene. Molecular structures are shown for each. Spectra are scaled and offset for clarity.

The SERS spectra of lycopene and β-carotene were highly similar, exhibiting prominent peaks at ~1154 cm^{-1} and ~1520 cm^{-1} (Figure 19). The largest spectral differences between the two are fluctuations in the shoulder peak near 1200 cm^{-1} and in the doublet near 1300 cm^{-1}, and an intensity and wavenumber shift of the peak near 1520 cm^{-1} (Figure 20). To analyze the carotenoid profile of carrot juice, tomato juice, and V8 juice blend, PC-SERS was performed on organic extracts from each product. For comparison, the PC-SERS protocol was also applied to lycopene and β-carotene references. Ethanol was used as the mobile phase for each sample (full spectral results can be found in , Appendix B). During elution, the β-carotene reference was seen to migrate with the solvent front as a faint yellow band, whereas the lycopene reference did not visibly move from its initial spot. Since the ethanol solubility of β-carotene is higher than that of lycopene, analyte partitioning in the mobile phase (i.e., solubility) is probably the major factor in this PC separation.

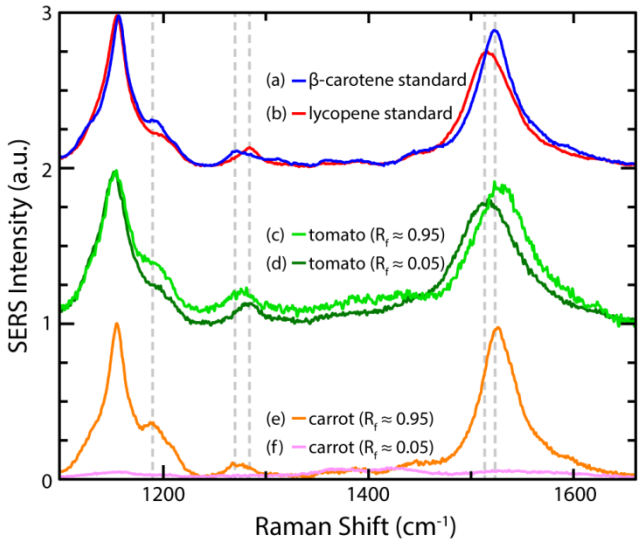

Figure 20. SERS spectra of β-carotene (a) and lycopene (b) on nanopaper, compared to PC-SERS spectra of tomato (c-d) and carrot (e-f). For clear comparison, (a-e) are offset and scaled with reference to the major carotenoid peak near 1154 cm^{-1}. Because (f) showed no carotenoid signal, it was instead scaled to match the background signal of (e). Vertical guides are placed where (a) and (b) exhibit the largest variation.

SERS intensity profiles based on the major carotenoid peak observed at 1154 cm^{-1} (Figure 21) revealed a strong spectral signal near $R_f = 0$ on the lycopene sample, and at $0.8 < R_f < 1$ on the β-carotene sample. Three additional PC-SERS replicates were performed for lycopene and β-carotene references to ensure repeatability (Figure 22), and each replicate's results were consistent with those found in Figure 21. Some weak signal was observed in the lycopene reference sample at $0.5 < R_f < 1$, which we believe to be the result of β-carotene contamination in our lycopene standard (see Appendix B for details). The SERS intensity profile for carrot juice extract showed localization of carotenoid peaks mostly at $0.8 < R_f < 1$. The tomato juice extract and the V8 extract both showed localization centered near $R_f = 0$ and, to a lesser extent, at $0.8 < R_f < 1$.

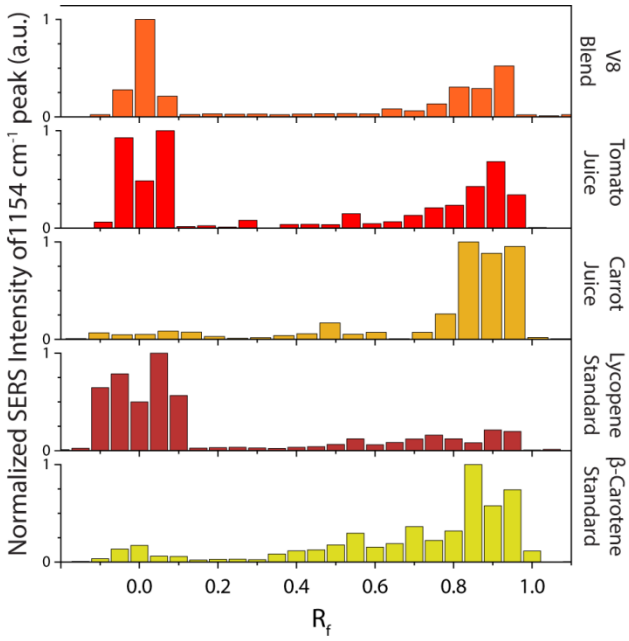

Figure 21. PC-SERS of juice extracts containing carotenoids, with lycopene and β-carotene references. Separation was performed on nanopaper, using absolute ethanol as the mobile phase. Intensities are relative to the nanopaper background signal at 900 cm^{-1}, and each profile is normalized from 0 to 1 for clarity. Total chromatogram length varies between samples; each bar represents 1 mm distance.

The results of Figure 21 imply that the major carotenoid identified in carrot juice was β-carotene, while tomato juice and V8 juice blend contained both lycopene and β-carotene. This was confirmed by examining individual spectra within SERS maps of the carrot and tomato extracts (Figure 20). The tomato spectrum collected from $R_f = 0.05$ exhibits a greater similarity to the lycopene reference spectrum, whereas the spectra at $R_f = 0.95$ are more similar to the β-carotene reference spectrum for both carrot and tomato juice extracts. The V8 PC-SERS results show the same trend.

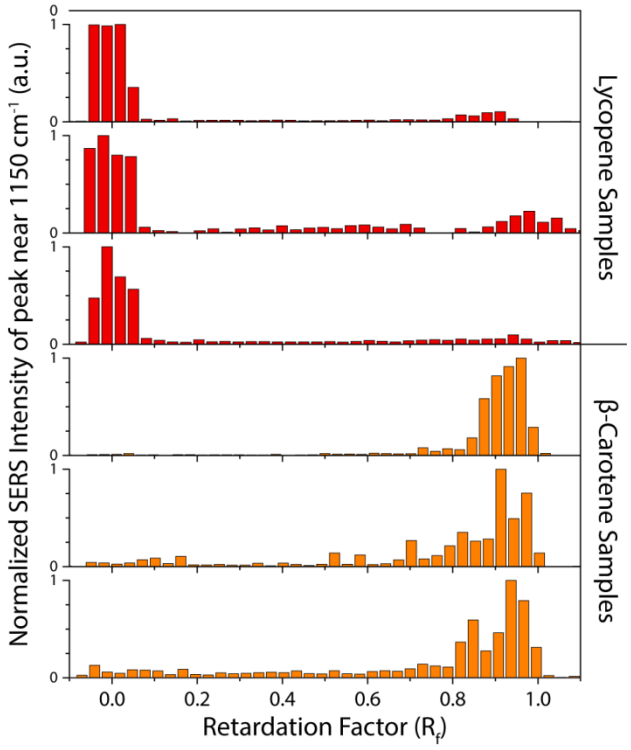

Figure 22. Additional PC-SERS results for carotenoid reference experiments. 3 additional replicates were performed for lycopene and β-carotene references, to demonstrate repeatability. Samples were prepared and analyzed in the same manner as those in Figure 21. Linear spatial resolution: 250 μm.

Chapter Conclusion

In conclusion, we have successfully synthesized a PC-SERS substrate, nanopaper, by performing the commonly known silver mirror reaction in the presence of glass microfiber filters. The synthesis is simple and scalable, resulting in a stable product that can be used as both a PC separation stationary phase and a SERS substrate. The utility of our nanopaper substrate was demonstrated by performing the separation and subsequent SERS identification of mixed organic dyes, as well as extracts from natural products. This demonstration showed the synergistic power of coupling PC separation with SERS detection; the PC separation simplified the SERS identification of mixed analytes, while the SERS identification simplified the interpretation of the PC separation. The low-cost, disposable, and portable nanopaper can serve

as a versatile technique for the identification of chemical and biological compounds within complex matrices.

CHAPTER IV

CONCLUSION AND FUTURE WORK

SERS is a powerful tool that overcomes the key disadvantage of Raman spectroscopy (low sensitivity) while inheriting its many advantages. A method for quantitative SERS analysis has been demonstrated for a particular kinetic assay, which was capable of accounting for variation in SERS enhancement factors. This quantitative method was implemented by covalently attaching a non-reactive internal standard (IS) to substrate surfaces and normalizing SERS spectra to the IS signal. This SERS platform was found to be a robust and sensitive method for quantitative analysis of kinetic assays, with potential applications in many fields.

A new SERS substrate was developed with the intent of simplifying sample preparation, SERS measurement, and results interpretation. The substrate, nanopaper, has an elegantly simple synthesis, making it accessible to researchers. It is robust, easily portable, and multifunctional. Nanopaper can be used as a simple SERS substrate, or through the simple elution of solvent through the paper it can be used as a coupled separation-detection method which increases the confidence of SERS identification.

I believe that the future prospects of this research are significant. My recent work with nanopaper (subsequent to the experiments of Chapter III) has revealed that it is even more versatile than indicated in Chapter III. In addition to simplifying SERS sample preparation, measurement, and interpretation, it is also a tool for sample collection. I have recently investigated the use of nanopaper as a swab, a dipstick, or even a filter to collect dusts, liquids, and vapor samples. Furthermore, contaminated samples can be collected with any of the above techniques and, because the substrate itself is chromatographically active, removing contaminant

effects is simple. Preliminary data indicate that sample collection and analysis with nanopaper is viable in a wide array of formats and for a wide array of substances.

Additional future work is also recommended to enable quantitative SERS with the nanopaper substrate. My preliminary studies have indicated that this should be possible by combining the ideas in Chapters II and III of this dissertation. Modifying nanopaper with an IS could allow quantitation of substances deposited onto the nanopaper. This modification could potentially have an additional benefit by allowing the surface properties of nanopaper to be tuned for optimal sample collection and/or chromatography performance. For example, fentanyl solution deposited on unmodified nanopaper was undetectable due to fentanyl's poor interaction with the surface; however, when deposited on nanopaper with an adsorbed monolayer of 1-butanethiol, fentanyl was easily detected.

Future work on this topic should take advantage of the versatile functions of nanopaper. To enable quantitative analysis with nanopaper, a protocol for modifying nanopaper surfaces must be standardized. Experiments should be performed to assess the effects of an IS adsorption layer on the SERS intensity of subsequently adsorbed analytes, and quantification performance should be evaluated. Different classes of IS (i.e., hydrophilic, hydrophobic, charged species) should be investigated to tune the surface properties. Finally, quantitation should be combined with the chromatography function to demonstrate quantitative PC-SERS.

To investigate the sample collection capabilities of nanopaper, each collection method should be tested. In particular, the filtration method seems the most interesting and useful. To evaluate this method, Raman-active chemical dusts could be mixed with a cutting agent (i.e. a powder mixture of 0.1 wt% R6G in lactose) and dispersed in a chamber equipped with a nanopaper-filtered vacuum outlet. Particle capture performance and SERS signal performance

could then be evaluated at different R6G loadings to determine a detection threshold. The platform could be extended to more complex mixtures by employing the PC-SERS protocol after filtration.

In conclusion, I believe that this body of work represents a significant advance in the field of chemical detection. In particular, the development of nanopaper and the possibilities for its future applications could be a milestone in SERS analysis for field-work and portable applications. The work is not yet finished, there is more to be discovered on this topic and with the nanopaper substrate.

REFERENCES

1 Skoog, D. A., Holler, F. J. & Crouch, S. R. *Principles of instrumental analysis. 6th ed*. (Belmont, Calif. : Thomson Brooks/Cole, [2007], 2007).

2 Le Ru, E. C. & Etchegoin, P. G. in *Principles of Surface-Enhanced Raman Spectroscopy* (eds Eric C. Le Ru & Pablo G. Etchegoin) 29-120 (Elsevier, 2009).

3 Kiefer, W. Recent Advances in linear and nonlinear Raman spectroscopy I. *Journal of Raman Spectroscopy* **38**, 1538-1553, doi:10.1002/jrs.1902 (2007).

4 Raman, C. V. & Krishnan, K. S. A New Type of Secondary Radiation. *Nature* **121**, 501, doi:10.1038/121501c0 (1928).

5 Haynes, C. L., McFarland, A. D. & Van Duyne, R. P. Surface-Enhanced Raman Spectroscopy. *Analytical Chemistry* **77**, 338 A-346 A, doi:10.1021/ac053456d (2005).

6 Kneipp, K., Kneipp, H., Itzkan, I., Dasari, R. R. & Feld, M. S. Ultrasensitive Chemical Analysis by Raman Spectroscopy. *Chemical Reviews* **99**, 2957-2976, doi:10.1021/cr980133r (1999).

7 Uriarte, L. M. *et al.* The self-absorption phenomenon in quantitative Raman spectroscopy and how to correct its effects. *Microchemical Journal* **139**, 134-138, doi:10.1016/j.microc.2018.02.013 (2018).

8 Lin-Vien, D. *The Handbook of infrared and raman characteristic frequencies of organic molecules. Daimay Lin-Vien [and others]*. (Boston : Academic Press, [1991], 1991).

9 Parker, F. S. *Applications of infrared, raman, and resonance raman spectroscopy in biochemistry. Frank S. Parker*. (New York : Plenum Press, [1983], 1983).

10 Haynes, C. L., Yonzon, C. R., Zhang, X. & Van Duyne, R. P. Surface-enhanced Raman sensors: early history and the development of sensors for quantitative biowarfare agent and glucose detection. *Journal of Raman Spectroscopy* **36**, 471-484, doi:10.1002/jrs.1376 (2005).

11 Fleischmann, M., Hendra, P. J. & McQuillan, A. J. Raman spectra of pyridine adsorbed at a silver electrode. *Chemical Physics Letters* **26**, 163-166, doi:10.1016/0009-2614(74)85388-1 (1974).

12 Moskovits, M. Surface-enhanced spectroscopy. *Reviews of Modern Physics* **57**, 783-826, doi:10.1103/RevModPhys.57.783 (1985).

13 Jeanmaire, D. L. & Van Duyne, R. P. Surface raman spectroelectrochemistry: Part I. Heterocyclic, aromatic, and aliphatic amines adsorbed on the anodized silver electrode.

Journal of Electroanalytical Chemistry and Interfacial Electrochemistry **84**, 1-20, doi:10.1016/S0022-0728(77)80224-6 (1977).

14 Albrecht, M. G. & Creighton, J. A. Anomalously intense Raman spectra of pyridine at a silver electrode. *Journal of the American Chemical Society* **99**, 5215-5217, doi:10.1021/ja00457a071 (1977).

15 Le Ru, E. C. & Etchegoin, P. G. in *Principles of Surface-Enhanced Raman Spectroscopy* (eds Eric C. Le Ru & Pablo G. Etchegoin) 1-27 (Elsevier, 2009).

16 Nie, S. & Emory, S. R. Probing Single Molecules and Single Nanoparticles by Surface-Enhanced Raman Scattering. *Science* **275**, 1102 (1997).

17 Kneipp, K. *et al.* Single Molecule Detection Using Surface-Enhanced Raman Scattering (SERS). *Physical Review Letters* **78**, 1667-1670, doi:10.1103/PhysRevLett.78.1667 (1997).

18 Le Ru, E. C. & Etchegoin, P. G. in *Principles of Surface-Enhanced Raman Spectroscopy* (eds Eric C. Le Ru & Pablo G. Etchegoin) 185-264 (Elsevier, 2009).

19 Campion, A. & Kambhampati, P. Surface-enhanced Raman scattering. *Chemical Society Reviews* **27**, 241-250, doi:10.1039/A827241Z (1998).

20 Sharma, B., Frontiera, R. R., Henry, A.-I., Ringe, E. & Van Duyne, R. P. SERS: Materials, applications, and the future. *Materials Today* **15**, 16-25, doi:10.1016/S1369-7021(12)70017-2 (2012).

21 Cao, Y. *et al.* Engineering of SERS Substrates Based on Noble Metal Nanomaterials for Chemical and Biomedical Applications. *Applied Spectroscopy Reviews* **50**, 499-525, doi:10.1080/05704928.2014.923901 (2015).

22 Tiwari, V. S. *et al.* Non-resonance SERS effects of silver colloids with different shapes. *Chemical Physics Letters* **446**, 77-82, doi:10.1016/j.cplett.2007.07.106 (2007).

23 Sharma, B. *et al.* High-performance SERS substrates: Advances and challenges. *MRS Bulletin* **38**, 615-624, doi:10.1557/mrs.2013.161 (2013).

24 Mosier-Boss, P. A. Review of SERS Substrates for Chemical Sensing. *Nanomaterials* **7**, 142, doi:10.3390/nano7060142 (2017).

25 Li, W., Zhao, X., Yi, Z., Glushenkov, A. M. & Kong, L. Plasmonic substrates for surface enhanced Raman scattering. *Analytica Chimica Acta* **984**, 19-41, doi:10.1016/j.aca.2017.06.002 (2017).

26 Betz, J. F., Yu, W. W., Cheng, Y., White, I. M. & Rubloff, G. W. Simple SERS substrates: powerful, portable, and full of potential. *Physical Chemistry Chemical Physics* **16**, 2224-2239, doi:10.1039/C3CP53560F (2014).

27 Sackmann, M. & Materny, A. Surface enhanced Raman scattering (SERS)—a quantitative analytical tool? *Journal of Raman Spectroscopy* **37**, 305-310, doi:10.1002/jrs.1443 (2006).

28 Cialla, D. *et al.* Surface-enhanced Raman spectroscopy (SERS): progress and trends. *Analytical and Bioanalytical Chemistry* **403**, 27-54, doi:10.1007/s00216-011-5631-x (2012).

29 Yu, W. W. & White, I. M. Chromatographic separation and detection of target analytes from complex samples using inkjet printed SERS substrates. *Analyst* **138**, 3679-3686, doi:10.1039/C3AN00673E (2013).

30 McNay, G., Eustace, D., Smith, W. E., Faulds, K. & Graham, D. Surface-Enhanced Raman Scattering (SERS) and Surface-Enhanced Resonance Raman Scattering (SERRS): A Review of Applications. *Appl. Spectrosc.* **65**, 825-837 (2011).

31 Stiles, P. L., Dieringer, J. A., Shah, N. C. & Duyne, R. P. V. Surface-Enhanced Raman Spectroscopy. *Annual Review of Analytical Chemistry* **1**, 601-626, doi:10.1146/annurev.anchem.1.031207.112814 (2008).

32 Hao, J. *et al.* SERS detection of arsenic in water: A review. *Journal of Environmental Sciences* **36**, 152-162, doi:10.1016/j.jes.2015.05.013 (2015).

33 McAughtrie, S., Faulds, K. & Graham, D. Surface enhanced Raman spectroscopy (SERS): Potential applications for disease detection and treatment. *Journal of Photochemistry and Photobiology C: Photochemistry Reviews* **21**, 40-53, doi:10.1016/j.jphotochemrev.2014.09.002 (2014).

34 Muehlethaler, C., Leona, M. & Lombardi, J. R. Review of Surface Enhanced Raman Scattering Applications in Forensic Science. *Analytical Chemistry* **88**, 152-169, doi:10.1021/acs.analchem.5b04131 (2016).

35 Bell, S. E. J. & Sirimuthu, N. M. S. Quantitative surface-enhanced Raman spectroscopy. *Chemical Society Reviews* **37**, 1012-1024, doi:10.1039/B705965P (2008).

36 Ou, Y., Wang, L.-Y., Zhu, L.-W., Wan, L.-S. & Xu, Z.-K. In-Situ Immobilization of Silver Nanoparticles on Self-Assembled Honeycomb-Patterned Films Enables Surface-Enhanced Raman Scattering (SERS) Substrates. *The Journal of Physical Chemistry C* **118**, 11478-11484, doi:10.1021/jp503166g (2014).

37 Fan, M., Andrade, G. F. S. & Brolo, A. G. A review on the fabrication of substrates for surface enhanced Raman spectroscopy and their applications in analytical chemistry. *Analytica Chimica Acta* **693**, 7-25, doi:10.1016/j.aca.2011.03.002 (2011).

38 Shen, W. *et al.* Reliable Quantitative SERS Analysis Facilitated by Core–Shell Nanoparticles with Embedded Internal Standards. *Angewandte Chemie International Edition* **54**, 7308-7312, doi:10.1002/anie.201502171 (2015).

39 Xia, L., Kim, N. H. & Kim, K. Stabilization of hydroxyl-group-terminated SERS-marker molecules on μAg particles by silanization. *Journal of Colloid and Interface Science* **306**, 50-55, doi:10.1016/j.jcis.2006.10.012 (2007).

40 Zhou, Y., Ding, R., Joshi, P. & Zhang, P. Quantitative surface-enhanced Raman measurements with embedded internal reference. *Analytica Chimica Acta* **874**, 49-53, doi:10.1016/j.aca.2015.03.016 (2015).

41 Tao, A., Sinsermsuksakul, P. & Yang, P. Polyhedral Silver Nanocrystals with Distinct Scattering Signatures. *Angewandte Chemie International Edition* **45**, 4597-4601, doi:10.1002/anie.200601277 (2006).

42 Wu, H.-J. *et al.* Membrane-protein binding measured with solution-phase plasmonic nanocube sensors. *Nat Meth* **9**, 1189-1191, doi:10.1038/nmeth.2211 (2012).

43 Yang, Y., Liu, J., Fu, Z.-W. & Qin, D. Galvanic Replacement-Free Deposition of Au on Ag for Core–Shell Nanocubes with Enhanced Chemical Stability and SERS Activity. *Journal of the American Chemical Society* **136**, 8153-8156, doi:10.1021/ja502472x (2014).

44 Reisner, L. A., Cao, A. & Pandya, A. K. An integrated software system for processing, analyzing, and classifying Raman spectra. *Chemometrics and Intelligent Laboratory Systems* **105**, 83-90, doi:10.1016/j.chemolab.2010.09.011 (2011).

45 Johnson, P. B. & Christy, R. W. Optical Constants of the Noble Metals. *Physical Review B* **6**, 4370-4379 (1972).

46 Daimon, M. & Masumura, A. Measurement of the refractive index of distilled water from the near-infrared region to the ultraviolet region. *Appl. Opt.* **46**, 3811-3820, doi:10.1364/AO.46.003811 (2007).

47 Rheims, J., Köser, J. & Wriedt, T. Refractive-index measurements in the near-IR using an Abbe refractometer. *Measurement Science and Technology* **8**, 601 (1997).

48 Gaussian 09 (Gaussian, Inc., Wallingford, CT, 2009).

49 Liu, G. Z. *et al.* Electrochemical scanning tunneling microscopy examination of the structures of benzenethiol molecules adsorbed on Au(1 0 0) and Pt(1 0 0) electrodes. *Surface Science* **601**, 247-254, doi:10.1016/j.susc.2006.05.062 (2007).

50 Zhang, J. *et al.* Two-Dimensional Cysteine and Cystine Cluster Networks on Au(111) Disclosed by Voltammetry and in Situ Scanning Tunneling Microscopy. *Langmuir* **16**, 7229-7237, doi:10.1021/la000246h (2000).

51 Le Ru, E. C., Meyer, M., Blackie, E. & Etchegoin, P. G. Advanced aspects of electromagnetic SERS enhancement factors at a hot spot. *Journal of Raman Spectroscopy* **39**, 1127-1134, doi:10.1002/jrs.1945 (2008).

52 Le Ru, E. C., Etchegoin, P. G. & Meyer, M. Enhancement factor distribution around a single surface-enhanced Raman scattering hot spot and its relation to single molecule detection. *The Journal of Chemical Physics* **125**, 204701, doi:10.1063/1.2390694 (2006).

53 Kambhampati, P., Child, C. M., Foster, M. C. & Campion, A. On the chemical mechanism of surface enhanced Raman scattering: Experiment and theory. *The Journal of Chemical Physics* **108**, 5013-5026, doi:10.1063/1.475909 (1998).

54 Le Ru, E. C., Blackie, E., Meyer, M. & Etchegoin, P. G. Surface Enhanced Raman Scattering Enhancement Factors: A Comprehensive Study. *The Journal of Physical Chemistry C* **111**, 13794-13803, doi:10.1021/jp0687908 (2007).

55 Nielsen, A. T. & Houlihan, W. J. in *Organic Reactions* (John Wiley & Sons, Inc., 2004).

56 Ingold, C. K. *Structure and mechanism in organic chemistry*. 676-690 (Cornell University Press, 1953).

57 Koudelka, L. Aldol condensation of butanal in alkaline medium. Comparison of kinetic models. *Chemical Papers* **38**, 637-647 (1984).

58 Bruckner, R. in *Advanced Organic Chemistry* 129-167 (Academic Press, 2002).

59 Lavrich, D. J., Wetterer, S. M., Bernasek, S. L. & Scoles, G. Physisorption and Chemisorption of Alkanethiols and Alkyl Sulfides on Au(111). *The Journal of Physical Chemistry B* **102**, 3456-3465, doi:10.1021/jp980047v (1998).

60 Guthrie, J. P. Equilibrium constants for a series of simple aldol condensations, and linear free energy relations with other carbonyl addition reactions. *Canadian Journal of Chemistry* **56**, 962-973, doi:10.1139/v78-162 (1978).

61 Weatherston, J. D., Seguban, R. K. O., Hunt, D. & Wu, H.-J. Low-Cost and Simple Fabrication of Nanoplasmonic Paper for Coupled Chromatography Separation and Surface Enhanced Raman Detection. *ACS Sensors* **3**, 852-857, doi:10.1021/acssensors.8b00098 (2018).

62 Craig, A. P., Franca, A. S. & Irudayaraj, J. Surface-Enhanced Raman Spectroscopy Applied to Food Safety. *Annual Review of Food Science and Technology* **4**, 369-380, doi:10.1146/annurev-food-022811-101227 (2013).

63 Granger, J. H., Schlotter, N. E., Crawford, A. C. & Porter, M. D. Prospects for point-of-care pathogen diagnostics using surface-enhanced Raman scattering (SERS). *Chemical Society Reviews* **45**, 3865-3882, doi:10.1039/C5CS00828J (2016).

64 Nuntawong, N. *et al.* Trace detection of perchlorate in industrial-grade emulsion explosive with portable surface-enhanced Raman spectroscopy. *Forensic Science International* **233**, 174-178, doi:10.1016/j.forsciint.2013.09.012 (2013).

65 Zhiqiang, Z. *et al.* Highly reproducible surface-enhanced Raman scattering substrate for detection of phenolic pollutants. *Nanotechnology* **27**, 455301 (2016).

66 Ding, S.-Y., You, E.-M., Tian, Z.-Q. & Moskovits, M. Electromagnetic theories of surface-enhanced Raman spectroscopy. *Chemical Society Reviews* **46**, 4042-4076, doi:10.1039/C7CS00238F (2017).

67 Weatherston, J. D., Worstell, N. C. & Wu, H.-J. Quantitative surface-enhanced Raman spectroscopy for kinetic analysis of aldol condensation using Ag-Au core-shell nanocubes. *Analyst* **141**, 6051-6060, doi:10.1039/C6AN01098A (2016).

68 Zhang, X. *et al.* Ultrasensitive SERS Substrate Integrated with Uniform Subnanometer Scale "Hot Spots" Created by a Graphene Spacer for the Detection of Mercury Ions. *Small* **13**, 1603347-n/a, doi:10.1002/smll.201603347 (2017).

69 Driskell, J. D. *et al.* Rapid microRNA (miRNA) detection and classification via surface-enhanced Raman spectroscopy (SERS). *Biosensors and Bioelectronics* **24**, 917-922, doi:10.1016/j.bios.2008.07.060 (2008).

70 Jarvis, R. M. & Goodacre, R. Discrimination of Bacteria Using Surface-Enhanced Raman Spectroscopy. *Analytical Chemistry* **76**, 40-47, doi:10.1021/ac034689c (2004).

71 Shanmukh, S. *et al.* Identification and classification of respiratory syncytial virus (RSV) strains by surface-enhanced Raman spectroscopy and multivariate statistical techniques. *Analytical and Bioanalytical Chemistry* **390**, 1551-1555, doi:10.1007/s00216-008-1851-0 (2008).

72 Dass, C. *Fundamentals of Contemporary Mass Spectrometry*. 151-194 (John Wiley & Sons, Inc., 2007).

73 Han, X. X. *et al.* Analytical Technique for Label-Free Multi-Protein Detection Based on Western Blot and Surface-Enhanced Raman Scattering. *Analytical Chemistry* **80**, 2799-2804, doi:10.1021/ac702390u (2008).

74 Hobro, A. J. & Lendl, B. in *Surface Enhanced Raman Spectroscopy* 155-171 (Wiley-VCH Verlag GmbH & Co. KGaA, 2010).

75 Subaihi, A. *et al.* Quantitative Online Liquid Chromatography–Surface-Enhanced Raman Scattering (LC-SERS) of Methotrexate and its Major Metabolites. *Analytical Chemistry* **89**, 6702-6709, doi:10.1021/acs.analchem.7b00916 (2017).

76 Wallace, R. A., Lavrik, N. V. & Sepaniak, M. J. Ultra-thin layer chromatography with integrated silver colloid-based SERS detection. *ELECTROPHORESIS* **38**, 361-367, doi:10.1002/elps.201600319 (2017).

77 Zhu, Q., Cao, Y., Cao, Y., Chai, Y. & Lu, F. Rapid on-site TLC–SERS detection of four antidiabetes drugs used as adulterants in botanical dietary supplements. *Analytical and Bioanalytical Chemistry* **406**, 1877-1884, doi:10.1007/s00216-013-7605-7 (2014).

78 Block, R. J., Strange, R. L. & Zweig, G. *Paper Chromatography: A Laboratory Manual*. (Elsevier Science, 2013).

79 Jung, H., Park, M., Kang, M. & Jeong, K.-H. Silver nanoislands on cellulose fibers for chromatographic separation and ultrasensitive detection of small molecules. *Light Sci Appl* **5**, e16009, doi:10.1038/lsa.2016.9 (2016).

80 Zhang, K., Qing, J., Gao, H., Ji, J. & Liu, B. Coupling shell-isolated nanoparticle enhanced Raman spectroscopy with paper chromatography for multi-components on-site analysis. *Talanta* **162**, 52-56, doi:10.1016/j.talanta.2016.10.020 (2017).

81 Zhao, Y. *et al.* Dense AuNP/MoS2 hybrid fabrication on fiber membranes for molecule separation and SERS detection. *RSC Advances* **7**, 36516-36524, doi:10.1039/C7RA05568D (2017).

82 Jeffers, R. B. & Cooper, J. B. FT-Surface-Enhanced Raman Scattering of Phenylalanine Using Silver-Coated Glass Fiber Filters. *Spectroscopy Letters* **43**, 220-225, doi:10.1080/00387010903287102 (2010).

83 Rycenga, M. *et al.* Controlling the Synthesis and Assembly of Silver Nanostructures for Plasmonic Applications. *Chemical Reviews* **111**, 3669-3712, doi:10.1021/cr100275d (2011).

84 Saito, Y., Wang, J. J., Batchelder, D. N. & Smith, D. A. Simple Chemical Method for Forming Silver Surfaces with Controlled Grain Sizes for Surface Plasmon Experiments. *Langmuir* **19**, 6857-6861, doi:10.1021/la0301240 (2003).

85 Saito, Y., Wang, J. J., Smith, D. A. & Batchelder, D. N. A Simple Chemical Method for the Preparation of Silver Surfaces for Efficient SERS. *Langmuir* **18**, 2959-2961, doi:10.1021/la011554y (2002).

86 Rodriguez, G. A. Extraction, Isolation, and Purification of Carotenoids. *Current Protocols in Food Analytical Chemistry* **00**, F2.1.1-F2.1.8, doi:10.1002/0471142913.faf0201s00 (2001).

87 Fiedor, J. & Burda, K. Potential Role of Carotenoids as Antioxidants in Human Health and Disease. *Nutrients* **6**, 466-488, doi:10.3390/nu6020466 (2014).

88 Barba, A. I. O., Hurtado, M. C., Mata, M. C. S., Ruiz, V. F. & Tejada, M. L. S. d. Application of a UV–vis detection-HPLC method for a rapid determination of lycopene and β-carotene in vegetables. *Food Chemistry* **95**, 328-336, doi:10.1016/j.foodchem.2005.02.028 (2006).

APPENDIX A

VIBRATIONAL CHARACTERIZATION*

DFT calculations

Density functional theory (DFT) calculations were carried out on NTP, MTBH, and 4-(4-methylthiophenyl)-3-buten-2-one adsorbed on Au surfaces, using the hybrid exchange-correlation functional B3LYP. Gold surfaces were represented by a cluster of 5 Au atoms in the case of NTP and 6 Au atoms in the case of MTBH and 4-(4-methylthiophenyl)-3-buten-2-one. The 6-311+G** basis set was used for C, H, O, N, S atoms. The modified LANL2DZ basis set was used for Au valence electrons and the corresponding relativistic core potentials were used for Au inner shell electrons. The solvent effects of ethanol were included by using the integral equation formalism polarization continuum model (IEFPCM). The molecule geometries were optimized (Figure 23), after which the Raman scattering frequencies and activities were calculated. The Raman spectra were expanded by a Lorenzian expansion with a FWHM of 10 cm^{-1} (Figure 24).

*Reproduced with permission from Weatherston, J. D., Worstell, N. C. & Wu, H.-J. Quantitative surface-enhanced Raman spectroscopy for kinetic analysis of aldol condensation using Ag-Au core-shell nanocubes. *Analyst 141*, 6051-6060, doi:10.1039/C6AN01098A (2016).

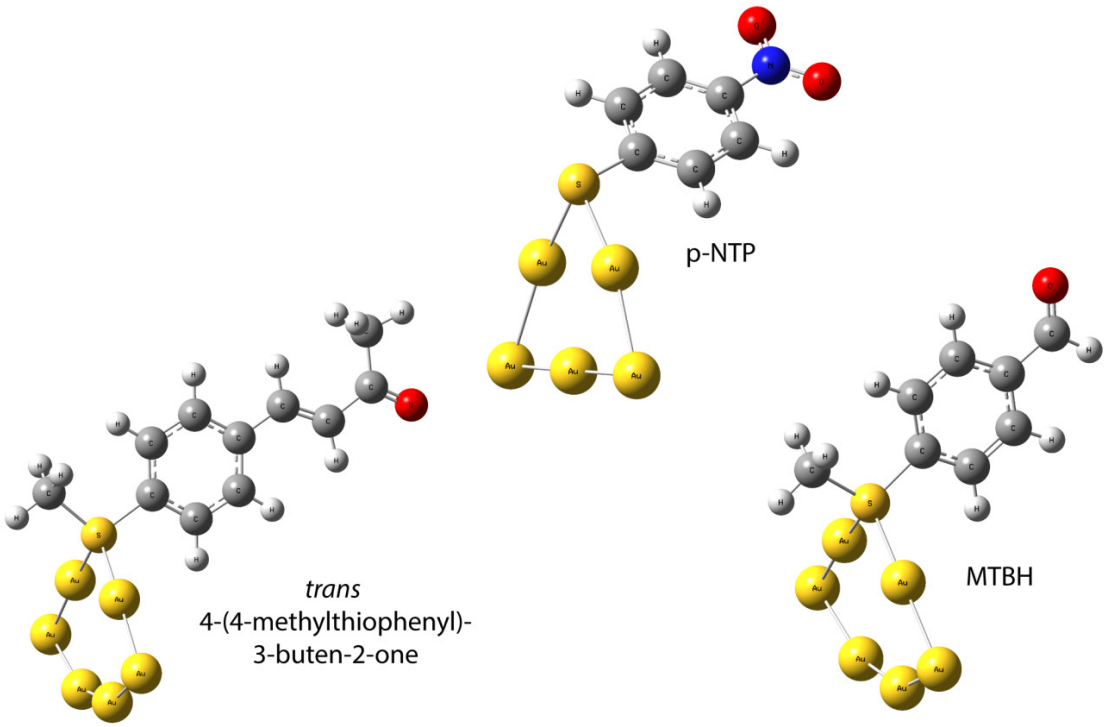

Figure 23. Optimized geometries from DFT calculations on molecules involved in the aldol condensation reaction.

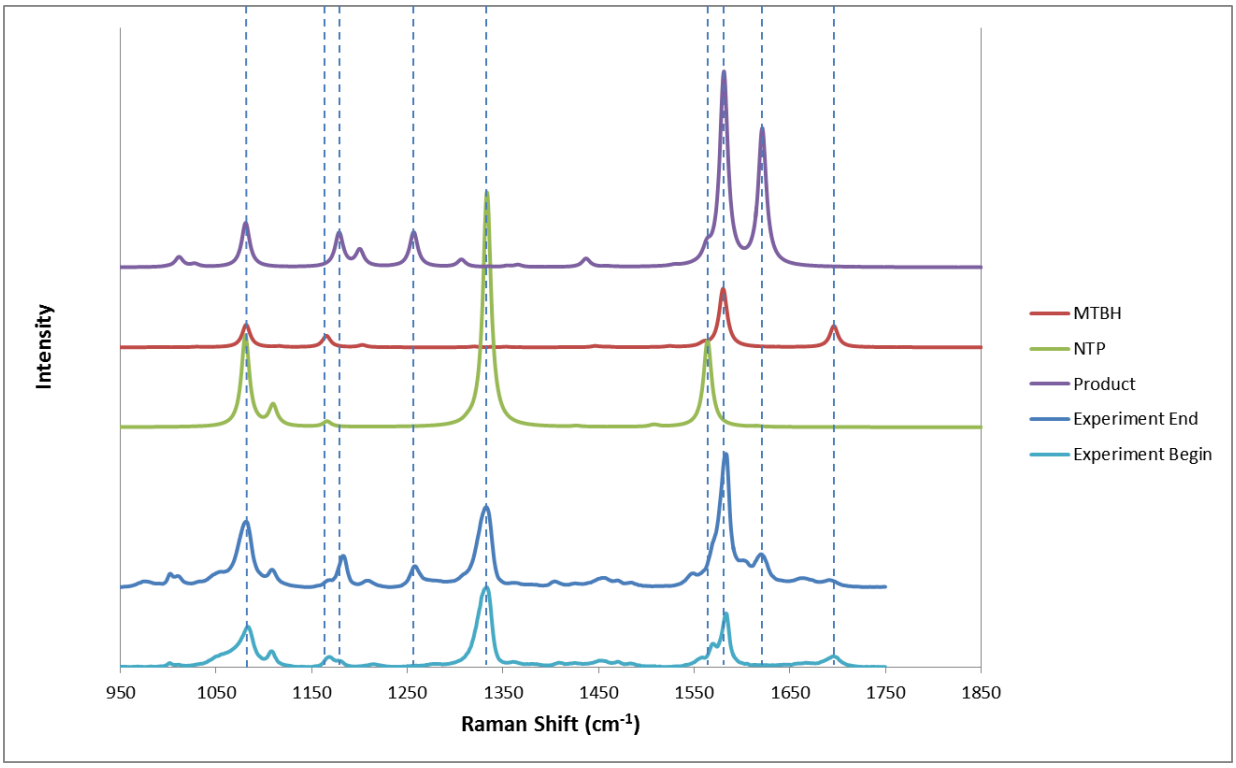

Figure 24. Simulated spectra for the three surface-adsorbed species present in the aldol condensation reaction (MTBH, NTP, Product). Calculated frequencies were scaled by a factor of 0.981 and offset for visual clarity. The IS-normalized experimental spectra of the first and last time points of an aldol condensation reaction are shown for comparison, again offset for clarity. Dashed lines are vertical guides to the eye.

APPENDIX B

SPECTRAL DATA SUPPORTING CHAPTER III*

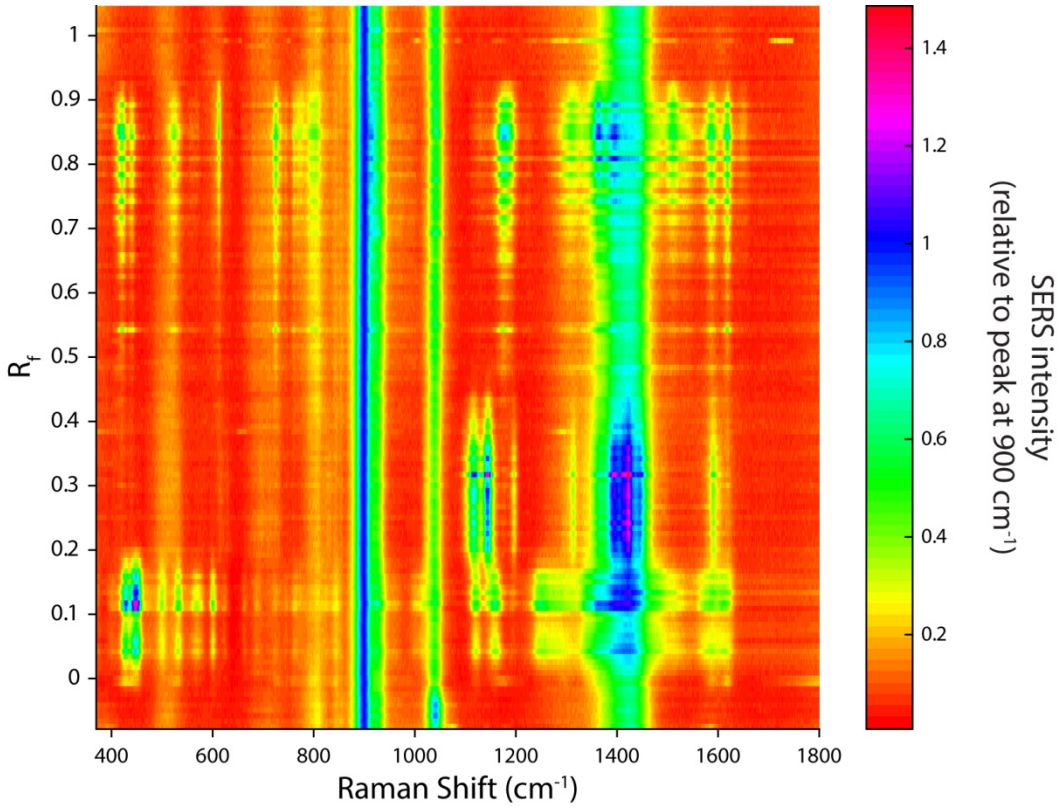

Figure 25. PC-SERS mapping results of 4 dyes on nanopaper. Colormap of SERS intensity (relative to nanopaper background peak at 900 cm^{-1}) showing spectral pattern vs location on the chromatogram. Linear spatial resolution: 250 µm.

* Reproduced with permission from Weatherston, J. D., Seguban, R. K. O., Hunt, D. & Wu, H.-J. Low-Cost and Simple Fabrication of Nanoplasmonic Paper for Coupled Chromatography Separation and Surface Enhanced Raman Detection. *ACS Sensors* 3, 852-857, doi:10.1021/acssensors.8b00098 (2018). Copyright 2018 American Chemical Society

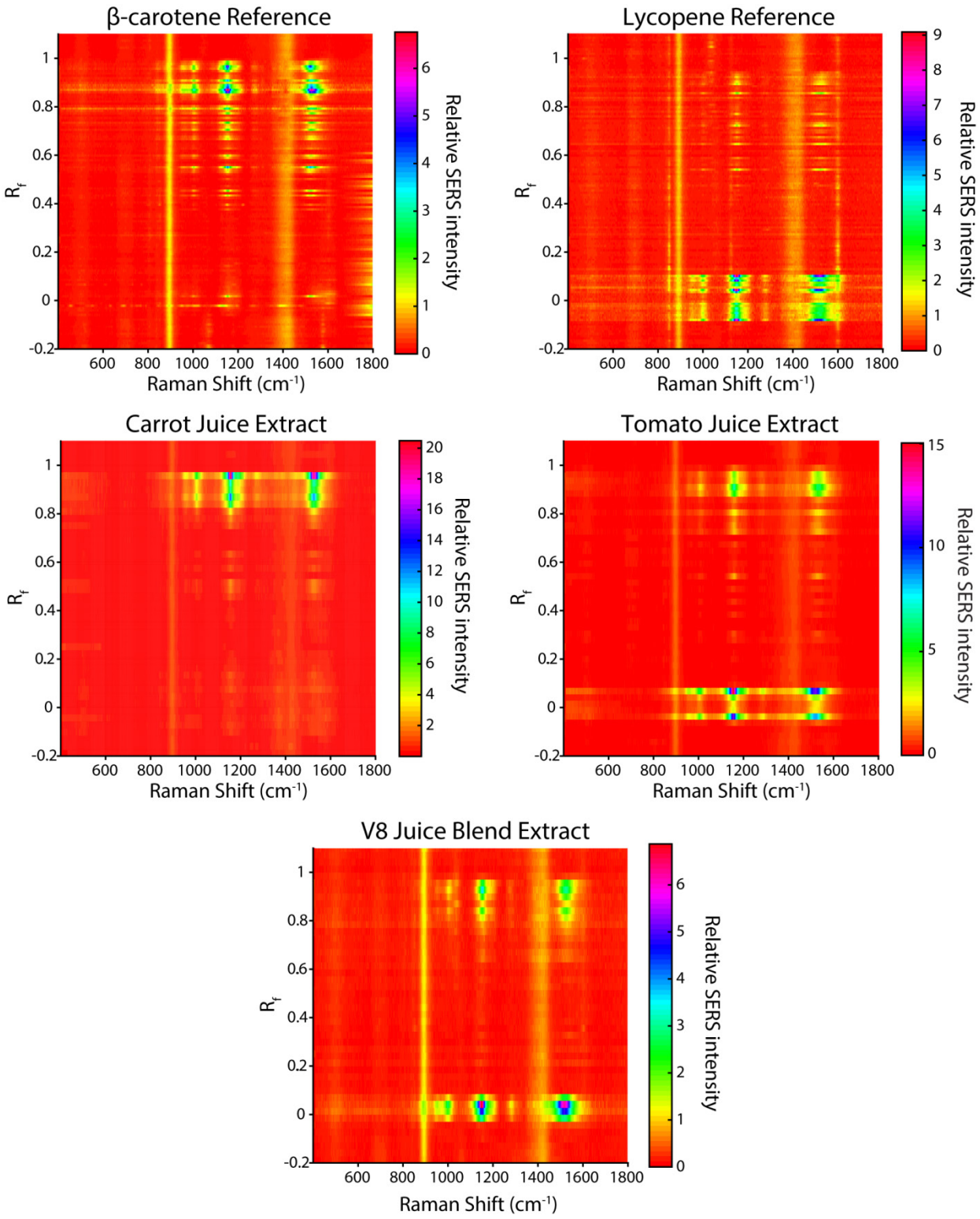

Figure 26. PC-SERS mapping results for carotenoid experiments. Colormap of SERS intensity (relative to nanopaper background peak at 900 cm^{-1}). Linear spatial resolution: 250 μm for references, 500 μm for extracts.

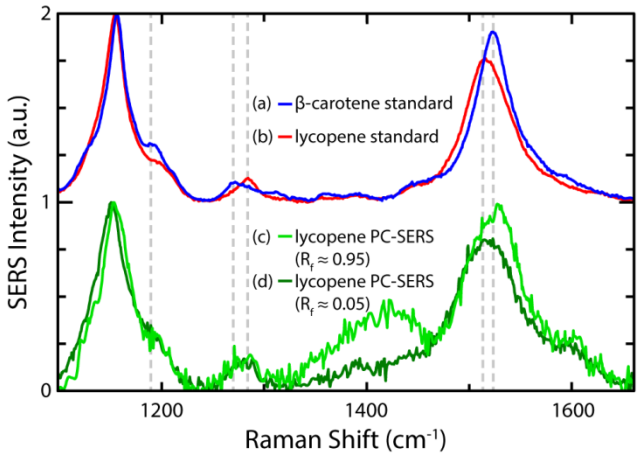

Figure 27. Evidence of lycopene contamination by other carotenoid. SERS spectra of β-carotene (a) and lycopene (b) references spotted on nanopaper; PC-SERS spectra from $R_f = 0.95$ (c) and $R_f = 0.05$ (d) of reference lycopene developed in ethanol. The peak shifts between (c) and (d) resemble the shifts between (a) and (b), particularly in the 1500cm^{-1}–1550 cm^{-1} region.